


# Identification of natural product 3, 5-diiodotyrosine as APOBEC3B inhibitor to prevent somatic mutation accumulation and cancer progression

Chunxia Chen,<sup>1</sup> Xinghua Sui,<sup>2</sup> Haoming Ning,<sup>1</sup> Yixuan Sun,<sup>1</sup> Jiangfeng Du,<sup>1,3</sup> Xiaotong Chen,<sup>1</sup> Xiuman Zhou,<sup>2</sup> Guanyu Chen,<sup>2</sup> Wenhui Shen,<sup>2</sup> Liwei Pang,<sup>1</sup> Xiaowen Zhou,<sup>1</sup> Ranran Shi,<sup>1</sup> Wanqiong Li,<sup>2</sup> Hongfei Wang,<sup>4</sup> Wenshan Zhao,<sup>1,5</sup> Wenjie Zhai,<sup>1,5</sup> Yuanming Qi,<sup>1,5</sup> Yahong Wu,<sup>1,3</sup> Yanfeng Gao <sup>1,2</sup>

**To cite:** Chen C, Sui X, Ning H, *et al.* Identification of natural product 3, 5-diiodotyrosine as APOBEC3B inhibitor to prevent somatic mutation accumulation and cancer progression. *Journal for ImmunoTherapy of Cancer* 2022;**10**:e005503. doi:10.1136/jitc-2022-005503

► Additional supplemental material is published online only. To view, please visit the journal online (<http://dx.doi.org/10.1136/jitc-2022-005503>).

Accepted 10 October 2022



© Author(s) (or their employer(s)) 2022. Re-use permitted under CC BY-NC. No commercial re-use. See rights and permissions. Published by BMJ.

For numbered affiliations see end of article.

## Correspondence to

Professor Yanfeng Gao; [gaoyf29@mail.sysu.edu.cn](mailto:gaoyf29@mail.sysu.edu.cn)

Dr Yahong Wu; [yahongwu@zzu.edu.cn](mailto:yahongwu@zzu.edu.cn)

## ABSTRACT

**Background** The development of cancer is largely dependent on the accumulation of somatic mutations, indicating the potential to develop cancer chemoprevention agents targeting mutation drivers. However, ideal cancer chemoprevention agents that can effectively inhibit the mutation drivers have not been identified yet.

**Methods** The somatic mutation signatures and expression analyses of APOBEC3B were performed in patient with pan-cancer. The computer-aided screening and skeleton-based searching were performed to identify natural products that can inhibit the activity of APOBEC3B. 4-nitroquinoline-1-oxide (4-NQO)-induced spontaneous esophageal squamous cell carcinoma (ESCC) and azoxymethane/dextran sulfate sodium (AOM/DSS)-induced spontaneous colon cancer mouse models were conducted to investigate the influences of APOBEC3B inhibitor on the prevention of somatic mutation accumulation and cancer progression.

**Results** Here, we discovered that the cytidine deaminase APOBEC3B correlated somatic mutations were widely observed in a variety of cancers, and its overexpression indicated poor survival. SMC247 (3, 5-diiodotyrosine), as a source of kelp iodine without side effects, could strongly bind APOBEC3B ( $K_D=65$  nM) and effectively inhibit its deaminase activity ( $IC_{50}=1.69$   $\mu$ M). Interestingly, 3, 5-diiodotyrosine could significantly reduce the clusters of mutations, prevent the precancerous lesion progression, and prolong the survival in 4-NQO-induced spontaneous ESCC and AOM/DSS-induced spontaneous colon cancer mouse models. Furthermore, 3, 5-diiodotyrosine could reduce colitis, increase the proportion and function of T lymphocytes via IL-15 in tumor microenvironment. The synergistic cancer prevention effects were observed when 3, 5-diiodotyrosine combined with PD-1/PD-L1 blockade.

**Conclusions** This is the first prove-of-concept study to elucidate that the natural product 3, 5-diiodotyrosine could prevent somatic mutation accumulation and cancer progression through inhibiting the enzymatic activity of APOBEC3B. In addition, 3, 5-diiodotyrosine could reduce the colitis and increase the infiltration and function of T lymphocytes via IL-15 in tumor microenvironment. 3, 5-diiodotyrosine combined with PD-1/PD-L1 blockade could elicit synergistic cancer prevention effects,

## WHAT IS ALREADY KNOWN ON THIS TOPIC

⇒ A large proportion of human cancers are caused by the accumulation of somatic mutations. However, there are still no effective agents for inhibiting mutation drivers due to the lack of therapeutic targets and unclear mechanisms. This raises the question whether it is possible to identify a major endogenous driver and develop effective natural product inhibitors to prevent somatic mutations and cancer progression.

## WHAT THIS STUDY ADDS

⇒ In this study, we found that the overexpression of APOBEC3B was positively associated with poor prognosis, and its somatic mutation signatures were widely observed in pan-cancer. Our *in vitro* and *in vivo* studies demonstrated that the first natural product 3, 5-diiodotyrosine from kelp could strongly bind to APOBEC3B and inhibit its deaminase activity, reduce colitis and increase the infiltration and function of T lymphocytes via IL-15 in tumor microenvironment.

## HOW THIS STUDY MIGHT AFFECT RESEARCH, PRACTICE OR POLICY

⇒ As such, for the first time, our study revealed a previously unrecognized function of 3, 5-diiodotyrosine as an APOBEC3B inhibitor, which could be exploited to prevent cancer progression, potentially enhanced antitumor immunity and reduced the immune checkpoint inhibitors-associated colitis of immunotherapy.

indicating a novel strategy for both prevent the somatic mutation accumulation and the immune-suppressive microenvironment exacerbation.

## INTRODUCTION

Advances in next-generation sequencing have determined that a large proportion of human cancers are caused by the

accumulation of somatic mutations.<sup>1-3</sup> Epidemiological studies have shown that exogenous factors such as radiation, alcohol consumption, smoking, exposure to carcinogens and micronutrient deficiency may trigger genetic mutation and cancer occurrence.<sup>4-5</sup> Although some chemoprevention agents have been investigated, the overall benefits remain controversial due to the lack of therapeutic targets and unclear mechanism.<sup>6-7</sup> Wang *et al* reported that there was no significant effect on cause-specific or total mortality during multivitamin supplementation for 6 years or postintervention follow-up for 20 years in Linxian, China.<sup>8</sup> Limburg *et al* found that the intervention of selenomethionine or celecoxib for 10 months in subjects with esophageal squamous dysplasia did not inhibit the occurrence of ESCC in the high-risk subjects.<sup>9</sup> In addition, researchers have also tried to target genomic instability and mutations in tumors to prevent the progression of cancer. Poly (ADP-Ribose) polymerase 1 (PARP1) inhibitors have been developed to treat patients with breast cancer with somatic BRCA1/2 mutations. However, the clinical application of PARPi in cancer therapy was limited due to their low selectivity, weak affinity, adverse side effects, and so on.<sup>10</sup> Jiang *et al* summarized mechanisms of genomic instability induced by DNA damage response (DDR) alterations, and therapeutic strategies targeting genomic instability including the combination of DDR inhibitors with immune checkpoint inhibitors (ICIs).<sup>11</sup> However, these therapeutic strategies have also encountered great challenges, including immune-related toxicities, dose, and drug resistance.<sup>12</sup> Therefore, it is considered impossible and undruggable to prevent cancer progression through preventing the somatic mutation.

Different mutation processes usually produce different types of single base substitution (SBS) combinations, which was called 'SBS signature'.<sup>13</sup> The first major category of endogenous factors that cause DNA damage or mutation is the spontaneous deamination of methylcytosine in presence of 5'-CG dinucleotides, results in cytosine to thymine (C>T) mutations. The process occurs naturally over time and is associated with aging.<sup>14</sup> The second largest endogenous source of somatic mutation in cancer is attributed to the deamination of apolipoprotein B mRNA editing catalytic peptide family (APOBEC), which catalyzes cytosine to uracil, results in C>T or C>G mutations through the DNA repair process.<sup>15</sup> APOBEC family have 11 family members, including APOBEC1 (A1), APOBEC2 (A2), APOBEC3A-3H (3A, 3B, 3C, 3D, 3F, 3G, 3H), APOBEC4 (A4) and activation-induced cytidine deaminase (AID).<sup>16</sup> Although each member has different hotspot recognition motifs and expression profiles,<sup>17</sup> more and more genetic analysis results have shown that APOBEC3B is a putative mutation driver to initiate the main source of endogenous enzyme-driven somatic mutations in several cancer types.<sup>12 18</sup>

APOBEC3B is a cytidine deaminase located in human chromosome 22p that catalyzes C>T conversion,<sup>19</sup> which is the only deaminase member mainly located

in the nucleoplasm.<sup>20 21</sup> The ligand of APOBEC3B is the single-stranded DNA (ssDNA) that mainly caused by DNA damage and replication fork interruption.<sup>22 23</sup> APOBEC3B is rarely expressed in normal tissues, and its highly efficient nucleic acid editing activity could induce high frequency mutations in viral genes to resist retroviruses, retrotransposon and DNA viruses such as HIV, MMTV, HBV and HPV.<sup>1 20</sup> However, if APOBEC3B is overexpressed or abnormally activated, a large number of somatic mutations will occur, and lead to carcinogenesis.<sup>24</sup> Therefore, APOBEC3B may serve as a novel target to prevent somatic mutation and cancer progression. Barzak *et al* had designed ssDNA containing 2'-deoxy-zebularine (dZCC-oligo) and its analogs, which are similar to APOBEC3B substrate, could selectively inhibit APOBEC3B, but the feasibility has not been verified at cellular level and *in vivo* experiments.<sup>25 26</sup> In addition, oligonucleotide drugs still face the problems of plasma membrane penetration, nuclease degradation, off-target, chemo-dependent toxicity and effective delivery.<sup>27</sup> Moreover, APOBEC3B is localized in the nucleoplasm, so the development of small molecule inhibitors will be more valuable. Unfortunately, up to now, there are no ideal APOBEC3B small molecule inhibitors as cancer chemoprevention agents.

In the current study, we found that APOBEC3B was a significant mutation driver and over-expressed in many cancers. Computer-aided virtual screening was performed to obtain small molecule inhibitors of APOBEC3B from natural product library. Their APOBEC3B inhibition activity and structure-activity relationships were investigated. The antitumor activity and mechanism of these compounds were investigated both *in vitro* and *in vivo* by using 4-NQO-induced spontaneous ESCC and AOM/DSS-induced spontaneous colon cancer mouse models.<sup>28 29</sup> For the first time, our results discovered that the putative diet iodine supplement SMC247 (3, 5-diiodotyrosine) from kelp could significantly inhibit the mutation-driving activity of APOBEC3B, reduce the colitis, increase the infiltration and function of T lymphocyte via IL-15 in tumor microenvironment and prevent cancer progression, indicating that inhibition of APOBEC3B could be a novel strategy for cancer chemoprevention. Furthermore, considering the immune microenvironment exacerbation as PD-L1 upregulated gradually in the precancerous lesion aside from the mutation accumulation. In our previous study, we discovered the first orally available proteolysis-resistant D peptide OPBP-1, which could selectively bind programmed cell death 1 ligand 1 (PD-L1), block PD-1/PD-L1 interaction, and effectively inhibit tumor growth.<sup>30</sup> Therefore, the synergistic effects of 3, 5-diiodotyrosine combined with PD-1/PD-L1 blockade were also investigated.

## MATERIAL AND METHODS

### Mutation signature and gene analysis

Mutational data of pan-cancer from The Cancer Genome Atlas (TCGA) (<https://xenabrowser.net/datapages/>) were downloaded, and mutational signatures of pan-cancer were analyzed using R package 'MutationalPatterns' (R V.4.0.1). Alexandrov *et al* proposed 96 distinct signature patterns from the curated data generated by TCGA and the International Cancer Genome Consortium using non-negative matrix factorization.<sup>31</sup> The mutation patterns were summarized and characterized using 96 Catalogue Of Somatic Mutations In Cancer (COSMIC) mutational signatures (V.3.2) to identify specific activity on the genome. The cancer types include Bladder Cancer (BLCA), Cervical Cancer (CESC), Lung Squamous Cell Carcinoma (LUSC), Lung Adenocarcinoma (LUAD), Head and Neck Cancer (HNSC), Esophageal Squamous Carcinoma (ESCC), Breast Cancer (BRCA), Esophageal Cancer (ESCA), Kidney Clear Cell Carcinoma (KIRC), Ovarian Cancer (OV), Uterine Carcinosarcoma (UCS), Stomach Cancer (STAD), Sarcoma (SARC), Liver Cancer (LIHC), Rectal Cancer (READ), Prostate Cancer (PRAD), Large B-cell Lymphoma (DLBC), Bile Duct Cancer (CHOL), Colon Cancer (COAD), Endometrioid Cancer (UCEC), Glioblastoma (GBM), Adrenocortical Cancer (ACC), Ocular melanomas (UVM), Testicular Cancer (TGCT), Thymoma (THYM), and Thyroid Cancer (THCA).

The National Institutes of Gene Expression Omnibus (GEO) database (<https://www.ncbi.nlm.nih.gov/geo/>) was utilized to obtain the gene expression data of normal and tumor samples in ESCC. GSE20347 cohort contained 17 paired tumor and peritumor ESCC samples (probe set ID: 207158\_at for APOBEC1, 206160\_at for APOBEC2, 210873\_x\_at for APOBEC3A, 206632\_s\_at for APOBEC3B, 209584\_x\_at for APOBEC3C, 214994\_at for APOBEC3F, 204205\_at for APOBEC3G and 219841\_at for AICDA). GSE37182 cohort contained 88 tumor and 84 peritumor colon cancer samples (probe set ID: ILMN\_1813881 for APOBEC1, ILMN\_1719143 for APOBEC2, ILMN\_1680192 for APOBEC3A, ILMN\_2219466 for APOBEC3B, ILMN\_1675684 for APOBEC3C, ILMN\_1702706 for APOBEC3F, ILMN\_2232478 for APOBEC3G and ILMN\_2164164 for AICDA).

### Plasmid construction and protein purification

We constructed APOBEC3B into pET-28a-MBP vector. The plasmid pET-28a-MBP-APOBEC3B was transformed into the *Escherichia coli* (*E. coli*) competent cell BL21, and was induced by 0.5 mM Isopropyl- $\beta$ -D-thiogalactoside (IPTG) (Solarbio, I8070, China) and 100  $\mu$ g/mL ampicillin (Solarbio, A8180, China) at 16°C overnight. Cells were collected and then suspended in a purification buffer (50 mM Tris-Cl, 150 mM NaCl, 1 mM DTT, 1 mM EDTA and 1 mM ZnCl<sub>2</sub>). After ultrasonic crushing, protein in supernatant was separated by MBP separation

and purification column to obtain active APOBEC3B protein (1.34 mg/mL) for the following experiment.

### Virtual screening

The crystal structure of APOBEC3B with resolution of 1.90 Å (PDB ID: 5TD5) was downloaded from the RCSB Protein Data Bank (PDB) (<https://www.rcsb.org/>). Homology modeling was performed by using APOBEC3B crystal structure as a template to complete missing region and change mutation sites to obtain complete wild-type structure in the Molecular Operating Environment (MOE) software (V.2019.08, Chemical Computing Group, Canada). In homology modeling, model score was GB/VI, and refinement parameter was gradient limit to 0.5. Two structures were superimposed together through the program 'superimposition' in MOE software, and the total root mean square deviation (RMSD) value as well as the RMSD value for each residue were generated and validated. The wild-type structure of APOBEC3B was optimized by modifying amount of hydrogen, charge and performing protonation by protonate 3D procedure in MOE. The possible screening pocket and binding area were operated and determined by the Site Finder options in MOE. Natural compounds were selected as small molecule screening library containing 638 well-described and commercially available compounds. Before molecular docking, compounds underwent energy minimization to obtain 3D multiple conformers. Flexible docking (parameter: induced fit) was performed by MOE software. Then, the optimal conformer of each compound was obtained by screening program 'unique filter'. According to the overall score (S value), molecular weight, better docking pose and so on, the top 30 compounds were obtained for subsequent experimental verification. All compounds were purchased from commercial supplier (TargetMol, Shanghai, China), dissolved in DMSO (10 mM), and preserved at -80°C.

### Fluorescence-based ssDNA cytosine deamination assay

To screen compounds which could inhibit the deamination enzymatic activity of APOBEC3B, the cytosine deamination assay was performed.<sup>32</sup> The substrate ssDNA of APOBEC3B 5'-6-FAM-ATTATTATTATTCAAATGGA TTTATTATTATTATTATTATT-TAMRA-3' was synthesized by GENEWIZ (Suzhou, China). Various diluted compounds were added into a 384-well plate. Then, 15  $\mu$ L of APOBEC3B protein diluted in 150 mM NaCl, 50 mM Tris, 1 mM protease inhibitor (cOmplete, EDTA-free, EASYpack, Roche, 04693132001, Switzerland) and 1 mM PMSF (Solarbio, P0100, China) was added and mixed, and then incubated for 15 min at 37°C. The final concentration of APOBEC3B protein was 0.04  $\mu$ M. Then, 10 pmol ssDNA substrate and 0.02 units *E. coli* uracil DNA glycosylase (UDG) (NEB, M0280S, US) were added and then incubated for 2 hours at 37°C. 4 M NaOH was added into the reaction system, followed by shaking for about 1 min and incubating at 37°C for another 30 min. 2 M Tris-Cl and 4 M HCl were then added to neutralize the reaction

mixture. Deaminase activity was subsequently quantified using fluorescence scores on multi-functional microporous plate detector with excitation wavelength at 485 nm and emission wavelength at 525 nm. The negative control used in this assay was solvent without compounds, or compounds that have verified without inhibitory effects. Dose-response curves and  $IC_{50}$  values were determined by the Graphpad Prism V.8.0 software.

#### Tris-boric-EDTA-urea gel-based ssDNA cytosine deaminase activity assay

The Tris-boric-EDTA (TBE)-urea gel-based ssDNA cytosine deaminase assay was performed as described.<sup>20</sup>  $1 \times 10^6$  KYSE70 cells were collected and then lysed by a non-denaturing cell lysate buffer supplementing 1 mM PMSF. The ssDNA (5'-ATTATTATTATTCAAATGGATTATTATTTATTATTATTATTTT-fluorescein-3') of APOBEC3B was synthesized by Beijing Liuhe Huada Gene Technology. A 2  $\mu$ L different concentration (0, 0.001, 0.01, 0.1, 1, 10, 100  $\mu$ M) of 3, 5-diiodotyrosine was mixed with 15  $\mu$ L cell lysate and then incubated at 37°C for 15 min. Then, 0.4  $\mu$ M ssDNA, 1.75 units RNase A, 0.025 units UDG and 2  $\mu$ L 10 $\times$ UDG buffer were added into reaction system and incubated at 37°C for 2 hours. A 100 mM NaOH was added into above reaction mixtures and placed in the thermostat at 95°C (HNDTC-100, China) for 10 min. The reaction mixtures were separated using the 15% TBE-urea gel electrophoresis. Results were visualized by ECL system (Azure C600, USA).

#### Microscale thermophoresis

The affinity of 3, 5-diiodotyrosine to human APOBEC3B was tested by Microscale thermophoresis (MST) (NanoTemper Technologies, Germany). Human APOBEC3B protein was labeled using Red-NHS647 dye (NanoTemper Technologies, L001, Germany). 3, 5-diiodotyrosine was diluted into gradient concentrations. The equal volumes of 0.05  $\mu$ M human APOBEC3B protein labeled by Red-NHS647 dye and the gradient concentrations of 3, 5-diiodotyrosine were mixed and incubated at room temperature for 5 min. Then, the mixture was loaded onto capillary for further detection. Data were calculated and estimated by analysis software (MO. Affinity Analysis, V.2.2.4).<sup>33</sup>

#### Bacterial resequencing

The constructed prokaryotic vector of APOBEC3B was transformed into *Escherichia coli* to induce the genetic mutation during the proliferation. Considering the rapid amplification of bacteria, they were treated with Vehicle and 2  $\mu$ M 3, 5-diiodotyrosine for 3 days, with the supplement of 100  $\mu$ M zinc ion.<sup>34</sup> Finally, the genomic DNA was extracted to perform the bacteria resequencing (Shanghai Parsenol Biotechnology, Shanghai, China).

#### Real-time quantitative PCR

Total RNA was extracted from cultured cells or tissue samples using the RNA Extraction Kit (MiniBEST Universal RNA Extraction Kit, TaKaRa, 9767, Japan).

Purity and concentration of total RNA were evaluated by nucleic acid analyzer called Nanodrop ND-2000 (Thermo Fisher Scientific, USA). Then, RevertAid First Strand cDNA Synthesis Kit (Thermo Fisher Scientific, K1622, USA) was used for RNA reverse transcription according to manufacturer's instruction. Finally, by using LightCycler 480 SYBR Green I Master (Roche, 04707516001, Switzerland), the real-time quantitative PCR (qRT-PCR) assay was performed on the Roche LightCycler 480.<sup>35</sup> All primers for qRT-PCR were listed in online supplemental table S1. All results were normalized by GAPDH.

#### Animals and treatment

##### Spontaneous ESCC mouse model

Female C57BL/6J mice (6 weeks) were purchased from Vital River Laboratory Animal Technology (Beijing, China). All mice were housed in the SPF animal facility at room temperature with humidity of 40%–60% and light and dark cycle for 12 hours.<sup>33</sup> Experimental procedures and ethical consent were approved by the Ethics Committee Zhengzhou University (ZZU202003).

After mice acclimated for one week, they were given drinking water containing 100  $\mu$ g/mL 4-NQO (N8141, Sigma, USA). After induction for 16 weeks, mice were fed with sterilized pure water to form ESCC spontaneously. During the experiment, activity status, body weight, food and water intake behavior, and survival status of mice were observed and recorded every 2 days. At week 28, the 4-NQO-induced ESCC mice were randomly divided into three groups. Mice were treated intraperitoneally (*i.p.*) with 200  $\mu$ L normal saline (1% DMSO), 0.5 mg/kg or 2 mg/kg 3, 5-diiodotyrosine every 2 days for 2 weeks.

To study the chemoprevention effect of 3, 5-diiodotyrosine combined with peptide OPBP-1. At week 28, the 4-NQO-induced ESCC mice were randomly assigned, and were treated with 200  $\mu$ L normal saline (1% DMSO), 0.5 mg/kg 3, 5-diiodotyrosine, 0.5 mg/kg OPBP-1 and 3, 5-diiodotyrosine combined with OPBP-1 for 2 weeks (once every 2 days, *i.p.*), respectively.

At week 30, the esophagus tissues of mice were harvested and photographed under an anatomical microscope, and the number and length diameter of tumor lesions were recorded.

##### Spontaneous colon cancer mouse model

After mice acclimated for one week, a group of vehicle mice were separated and other mice were injected (*i.p.*) with 10 mg/kg AOM (A5486, Sigma, USA). After 1 week, the injected mice were divided into four groups and labeled as NS group, 3, 5-diiodotyrosine group, OPBP-1 group, and 3, 5-diiodotyrosine combined with OPBP-1 group. Above four groups of mice were given 2% DSS (160110, MP Biomedicals) in drinking water for one week and then normal water for 2 weeks. The cycle was repeated three times. Vehicle mice drank normal water and were not given AOM and DSS during the whole process. After 7 days of AOM administration in the first round, mice in the chemoprevention group were injected intraperitoneally

with 200  $\mu$ L normal saline, 0.5 mg/kg 3, 5-diiodotyrosine, 0.5 mg/kg OPBP-1 and 3, 5-diiodotyrosine combined with OPBP-1, respectively. At the end of experiment (10 weeks after injection with AOM), all mice were euthanized, and the colon tissues of mice were harvested and evaluated by counting the tumor number and length diameter under macroscopic observation.

### **In vivo toxicity analysis**

At the end of *in vivo* experiment, serum samples of each mouse were collected and used to test hepatic damage by aspartate aminotransferase (AST) and alanine aminotransferase (ALT) kit (Nanjing Jiancheng Biological Engineering Research Institute, C010-2-1, C009-2-1, China) according to the manufactures' instructions. The heart, liver, spleen, lung and kidney samples of each group were collected and fixed by 4% paraformaldehyde solution, and sent to the Wuhan Service Biotechnology company in China for H&E staining assay.

### **Mouse whole exome sequencing**

Genomic DNA was extracted from esophagus tissues of naive mice, 4-NQO-induced ESCC mice treated with 200  $\mu$ L normal saline or 0.5 mg/kg 3, 5-diiodotyrosine (once every 2 days for 2 weeks, *i.p.*). All samples were used to perform whole exome sequencing analysis. Esophagus tissue DNA from naive mice was used to filter out the background mutational noise, false positive mutations, and age-related mutations. The qualified DNA samples after verification were randomly broken into 150 bp-220 bp fragments by Covaris. SureSelect XT Mouse All Exon kit was applied to build and capture library.

The Illumina NextSeq platforms, greater than 100 $\times$  sequencing depth, were used to perform sequencing. To identify the multiple classes of genomic abnormalities, genomic data were processed using a proprietary bioinformatics pipeline. Specifically, the BWA algorithm of the haplotypcaller module of GATK4 software was adopted to obtain the comparison results between the reference genome and samples, and detected small insertions/deletions (InDel) and single-nucleotide substitutions (SNPs). The known InDel and SNP databases and the BaseRecalibrator module of GATK4 software were used to recalibrate the base quality to increase the accuracy of mutation detection. Only the mutation site with QD (ie, variation quality value divided by coverage depth) greater than 2 were retained to decrease the error rates of InDel and SNP detection. Finally, InDel and SNP results were annotated to Refseq and other databases using Annovar software. The genomic landscape of mouse treated with NS or 3, 5-diiodotyrosine was summarized and visualized using R package 'maftools'. The mutation patterns were fitted using R package 'MutationalPatterns' to identify components matching to the 96 COSMIC mutational signatures (V.3.2). The refitting procedure bootstrapped 1000 times to avoid signature misattribution. The relative contribution of each COSMIC signature for each sample was then plotted using the R package 'ggplot2'. The

mouse whole exome sequencing was performed by OE Biotech (Shanghai, China).

### **Ex vivo assays**

For intracellular cytokine staining experiment, single cells of spleen and lymph node of mice were stimulated by 20 ng/mL phorbol 12-Myristate 13-acetate (PMA, Sigma, P8139, USA) and 1  $\mu$ M ionomycin (Sigma, 407952-5 MG, USA) for 4 hours.<sup>36</sup> Cells were collected and then incubated with surface antibodies anti-CD3-PerCP-eFluor 710 (17A2) and anti-CD8 $\alpha$ -PE (53-6.7). After 30 min, cells were washed by PBS buffer (pH 7.2) and immobilized at room temperature. After another 30 min, 800  $\mu$ L permeabilization solution was added into cells. Antibody Anti-IFN- $\gamma$ -APC (XMG1.2) was added and then incubated with the cells for another 30 min. After the cells were washed, the proportion of IFN- $\gamma$ <sup>+</sup>CD8<sup>+</sup> T cells was determined by flow cytometry. All fluorescence activated cell sorter (FACS) antibodies in our research are purchased from eBioscience, USA.

### **Coculture assay**

Human peripheral blood mononuclear cells (PBMCs) from healthy donors were isolated using lymphocyte separation solution (TBD, LTS1077, China) according to the manufactures' instructions.<sup>33</sup> PBMCs were stained with 0.2  $\mu$ M carboxyfluorescein succinimidyl ester-activated (CFSE) (eBioscience, 65-0850-84, USA), and then activated with 100 units IL-2 (PeproTech, 200-02-100, USA), 1  $\mu$ g/mL anti-CD28 (CD28.2, eBioscience, USA), and 1  $\mu$ g/mL anti-CD3 (OKT3, eBioscience, USA) stimulatory antibodies. Subsequently, the activated PBMCs were seeded into 48-well plates (4 $\times$ 10<sup>5</sup> cells per well) and then cultured in vehicle medium and the supernatants of KYSE70 cells pretreated with or without 10  $\mu$ M 3, 5-diiodotyrosine for 48 hours. Above medium was Roswell Park Memorial Institute (RPMI) 1640 complete medium (Gibco, Grand Island, USA) supplemented with 100  $\mu$ g/mL streptomycin (Solarbio, China), 100 U/mL penicillin (Solarbio, China) and 10% fetal bovine serum (FBS, BI, USA). After cells were cultured for 3 days. The intracellular cytokine staining experiment were performed as described in *ex vivo* assay. The proliferation of CD8<sup>+</sup> T cells and proportion of IFN- $\gamma$ <sup>+</sup>CD8<sup>+</sup> T cells were analyzed by flow cytometry.

### **Transcriptome sequencing**

The equal number of KYSE70 cells were seeded into six-well plates. After cells were completely adherent, cells were divided into two groups: vehicle group and 3, 5-diiodotyrosine treated group. Cells in vehicle group were replaced with fresh RPMI 1640 complete medium, and cells in 3, 5-diiodotyrosine treated group were replaced with equal volume of RPMI 1640 complete medium containing 10  $\mu$ M 3, 5-diiodotyrosine. After 48 hours, cells were lysed, collected and sent to company for transcriptome sequencing on Illumina NovaSeq6000 platform. The quality control, library preparation,

sequencing and analysis processes were performed by OE Biotech (Shanghai, China). Three independent samples for each group were performed.

## ELISA

The supernatants of KYSE70 cells treated with or without 10  $\mu\text{M}$  3, 5-diiodotyrosine for 48 hours were collected, respectively. Human IL-7 ELISA kit (DAKEWEI, 1110702, China) and IL-15 ELISA kit (Invitrogen, 88-7620, USA) was used to detect the secretion levels of IL-7 and IL-15.

## Statistical analysis

GraphPad Prism (V.8) and R V.4.0.1 (<https://cran.r-project.org/>) were applied for statistical analysis. All data were displayed as means $\pm$ SEM. The survival curves were evaluated using the Kaplan-Meier method and the log-rank test. The means among groups were determined through Student's *t*-test or Wilcoxon test. Spearman's correlation analysis was adopted to evaluate the correlation between continuous variables. \* $p < 0.05$ , \*\* $p < 0.01$ , and \*\*\* $p < 0.001$  were regarded as statistical significance.

## RESULTS

### APOBEC3B was overexpressed in pan-cancer and positively associated with poor prognosis

In order to investigate the SBS mutational landscape, we analyzed the somatic mutation data of pan-cancer patients from TCGA and fitted the mutational patterns to 96 COSMIC mutational signatures. In addition to the exposure of some exogenous carcinogens, endogenous mutation drivers associated with single base substitution played important roles in the development and progression of cancer. As shown in [figure 1A](#), besides the age-related SBS1 signatures, SBS2 and SBS13 closely associated with APOBEC activity were the second and third ranked frequent mutation signatures, respectively. These results indicated that the APOBEC family might be the potential pan-cancer mutation driver.

Considering that esophageal squamous carcinoma (ESCC) and colon cancer belonged to typical epithelial cancer types with obvious APOBEC-driven mutation characteristics, we first analyzed the expression levels of APOBEC family members by using GEO database. Results in [figure 1B](#) showed that APOBEC3B expression in tumor tissues was the highest among APOBEC family members, and much higher than that in normal tissues. Then, we found that APOBEC3B expression in tumor tissues was higher than in normal tissues in other cancers as well (online supplemental figure S1). Furthermore, the Kaplan-Meier survival curve showed that the high expression of APOBEC3B was correlated with the poor prognosis in pan-cancer cohort ([figure 1C](#)). Burns *et al* reported that APOBEC3B was upregulated in multiple cancer types, and its mutation form accounted for a large proportion of both scattered and clustered mutations in a variety of distinct cancers.<sup>1</sup> These results suggested that

APOBEC3B may serve as a potential target to develop cancer chemoprevention agents.

### Screening of natural products as APOBEC3B inhibitors

The crystal structure of APOBEC3B (5TD5)<sup>37</sup> was used to obtain the corresponding homology model of wild type APOBEC3B structure by MOE software (online supplemental table S2 and figure S2A), because there were lots of mutation sites and missing regions in crystal structure of APOBEC3B (online supplemental figure S2B). The sequence identity was 87.9%, and the RMSD of overall heavy atom value between aligned regions of two structures was 0.32 Å (online supplemental figure S2C, D). RMSD values for each residue between homology model structure and template structure were less than 1 Å (online supplemental figure 2E). These results indicated that our homology modeling was successful and reliable, and could be used for subsequent virtual screening. Among proprietary druggable pockets predicted by Site Finder in MOE, we chose a pocket with size of 70 Å to screen compounds from natural product library (online supplemental figure S2F). Since this pocket not only demonstrated a standardized druggable size, but also located in the interface between the catalytic activity area and the substrate binding area of APOBEC3B. Finally, the top 30 compounds were selected for the *in vitro* bioassay test according to the process illustrated in [figure 2A](#). The docking results of 638 compounds with APOBEC3B were shown in online supplemental file 2 and the comprehensive workflow chart was summarized in online supplemental figure S3.

To evaluate whether these candidate compounds could inhibit the cytosine deamination activity of APOBEC3B, we performed fluorescence-based ssDNA cytosine deamination assay<sup>32</sup> and found that 10 compounds (100  $\mu\text{M}$ ) could inhibit the enzymatic activity with inhibition rate over 20% ([figure 2B,C](#) and online supplemental table S3). Furthermore, SMC130 was identified to effectively inhibit APOBEC3B activity with a dose-dependent manner and had a desired  $\text{IC}_{50}$  value of 6.93  $\mu\text{M}$  ([figure 2D](#)). Subsequently, we expected to seek compounds which are structurally similar to SMC130 and have stronger inhibitory activity. Skeleton similarity searching was conducted with SMC130 as the lead compound from the 638 natural products described above (online supplemental table S4). As a result, SMC247 (3, 5-diiodotyrosine) showed a more promising dose-dependent inhibitory activity with an  $\text{IC}_{50}$  of 1.69  $\mu\text{M}$  ([figure 2E](#)). After determining that 3, 5-diiodotyrosine could inhibit the cytosine deamination activity of APOBEC3B, its affinity to APOBEC3B was further detected by the MST assay. 3, 5-diiodotyrosine could strongly bind human APOBEC3B with a  $K_D$  value of 65 $\pm$ 40 nM ([figure 2F](#)).

We also evaluate the interaction between 3, 5-diiodotyrosine and APOBEC3B in cancer cells. KYSE150 cell line with low expression of APOBEC3B was selected (online supplemental figure S4A) for construction of a doxycycline (dox) inducible APOBEC3B overexpression

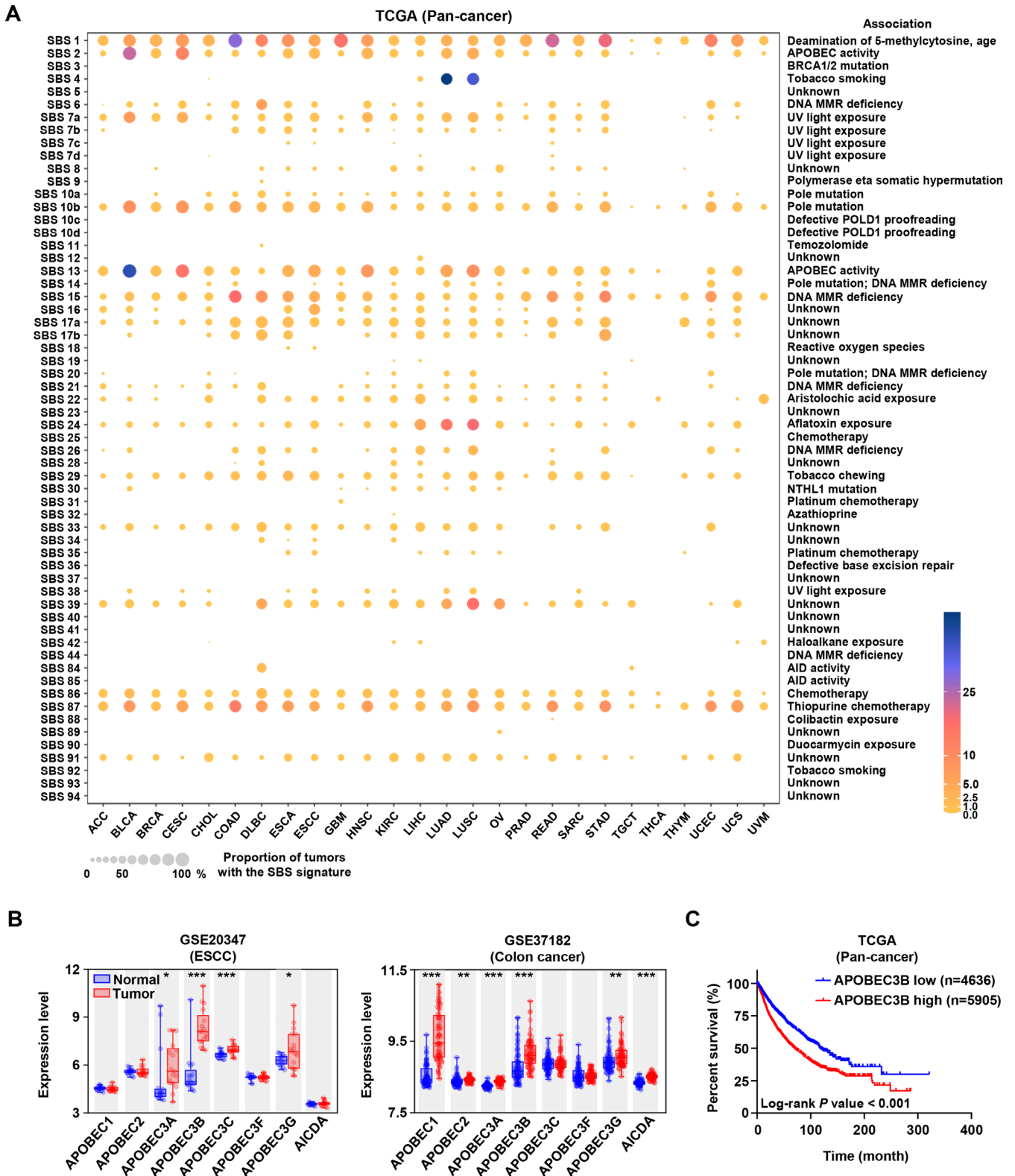


**Figure 1** The landscape of mutational signatures, expression and prognosis of APOBEC3B in pan-cancer. (A) The mutational signatures across pan-cancer from The Cancer Genome Atlas (TCGA) database. Cancer types were arranged as columns, and mutation signatures were displayed as rows. ‘Unknown’ represented mutation signatures that were unknown, unverified, or failed to be verified. MMR: mismatch repair. (B) Expression levels of APOBEC family members in normal and tumor tissues of human esophageal squamous carcinoma and colon cancer from Gene Expression Omnibus (GEO) database were analyzed. Data from GEO database have performed background correction and normalization by using the Robust Multiarray Average (RMA) algorithm in Bioconductor of R package, \* $p < 0.05$ , \*\* $p < 0.01$ , \*\*\* $p < 0.001$ . (C) Kaplan-Meier overall survival curve showed the relationship between APOBEC3B expression and pan-cancer patients’ overall survival ( $n = 4636$  for APOBEC3B-low and  $n = 5905$  for APOBEC3B-high based on receiver operating characteristic (ROC) curve analysis).

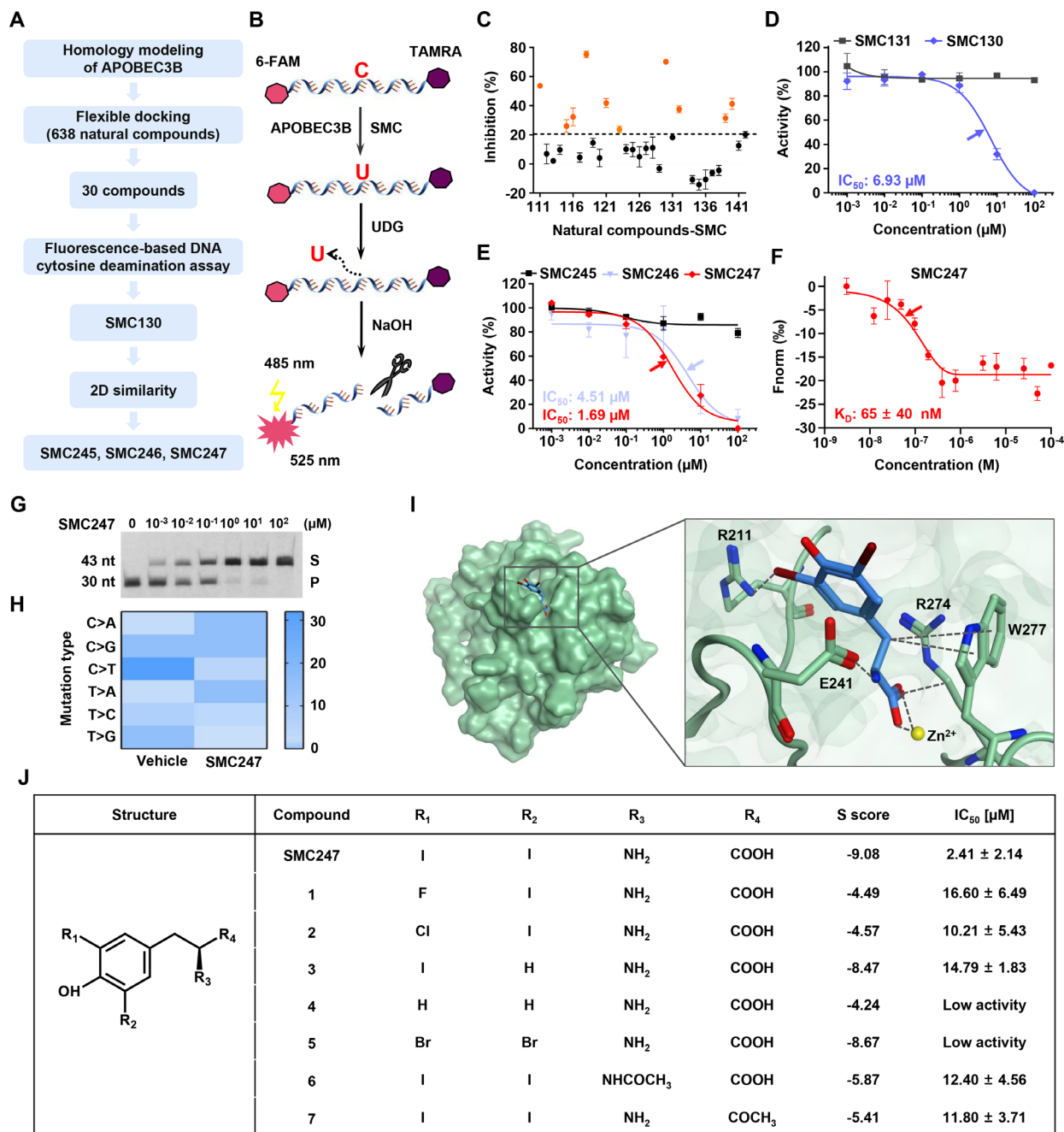


**Figure 2** Enzyme activity inhibitory of APOBEC3B and the structure and activity relationship of SMC247 (3, 5-diiodotyrosine). (A) Flowchart of molecule docking and experimental design to obtain inhibitors targeting APOBEC3B. (B) The principle of fluorescence-based DNA cytosine deamination assay. (C) The enzyme activity inhibitory rate (IR) of candidate compounds (100 μM). Ten compounds with IR >20% were labeled as orange. (D) The dose-dependent assay of SMC130. SMC131 represented a negative control with no inhibitory effect (black symbols). (E) The dose-dependent assay of SMC245, SMC246 and SMC247 obtained by two-dimensional similarity searching from NCI and zinc databases. The arrow showed the IC<sub>50</sub> concentration. (F) Dose response curve of SMC247 binding to APOBEC3B was examined by the MST assay. The K<sub>D</sub> value was calculated with analysis software (Mo. affinity analysis V.2.2.4). The arrow showed the K<sub>D</sub> concentration. (G) Analysis of APOBEC3B deaminase activity in KYSE70 cells with different concentrations of 3, 5-diiodotyrosine (S, substrate; P, product; nt: nucleotide). The 15 μL lysates of 1 × 10<sup>6</sup> KYSE70 cells were incubated with 2 μL different concentrations (0, 0.001, 0.01, 0.1, 1, 10, 100 μM) of 3, 5-diiodotyrosine. The ssDNA was added into above reaction system and used for substrate of APOBEC3B. NaOH was used to break the phosphodiester bond on uracil created by APOBEC3B mutation function. The reaction mixtures were separated and analyzed using the 15% TBE-urea gel electrophoresis. (H) The heat map of single nucleotide substitution in bacterial genomes after 3, 5-diiodotyrosine treatment. (I) The binding pattern of 3, 5-diiodotyrosine (blue) and APOBEC3B (green) was predicted by MOE software. The interactions were indicated in black dotted lines. The negative score indicated the affinity energy (S scores). The lower the S score, the higher the affinity energy. (J) The structure and activity relationship analysis of 3, 5-diiodotyrosine. Replaceable molecules were found based on the key groups (R<sub>1</sub>, R<sub>2</sub>, R<sub>3</sub>, R<sub>4</sub>). Data are representative of at least three independent experiments.



cell line KYSE150-APOBEC3B (online supplemental figure S4B). A 4ng/mL dox could induce APOBEC3B overexpression. Results in online supplemental figure S4C showed that 3, 5-diiodotyrosine had high affinity to KYSE150-APOBEC3B cells ( $K_D = 6.14 \pm 7.93 \mu\text{M}$ ), but it had no affinity to KYSE150-vector cells by MST assay. Furthermore, 3, 5-diiodotyrosine could strongly inhibit the deaminase activity of APOBEC3B in KYSE150-APOBEC3B cells (online supplemental figure S4D). These results further demonstrated that 3, 5-diiodotyrosine could interact with APOBEC3B and inhibit the deaminase activity of APOBEC3B.

Further, the TBE-urea gel-based ssDNA cytosine assay was performed to evaluate the DNA-binding ability after APOBEC3B interacted with 3, 5-diiodotyrosine. As shown in figure 2G, the product amount was reduced in a dose-dependent manner after treatment with 3, 5-diiodotyrosine, and the deaminase activity of APOBEC3B was significantly inhibited when 3, 5-diiodotyrosine (1  $\mu\text{M}$ ) incubated with KYSE70 cell lysates for 15 min, which further illustrated that 3, 5-diiodotyrosine could inhibit the binding ability of APOBEC3B to substrate ssDNA and inhibit the deamination function of APOBEC3B.

To validate the specificity of 3, 5-diiodotyrosine to APOBEC3B, APOBEC3A, and APOBEC3G protein, the homologous family members of APOBEC3B, were randomly chosen. Results in online supplemental figure S5A, C showed that 3, 5-diiodotyrosine weakly bound to APOBEC3A and APOBEC3G. When the concentration of 3, 5-diiodotyrosine reached 100  $\mu\text{M}$ , the inhibition rates of APOBEC3A and APOBEC3G deaminase activity were still less than 50% (online supplemental figure S5B, D). The detailed ssDNA sequences were shown in online supplemental table S5. These results indicated that 3, 5-diiodotyrosine could specifically bind to APOBEC3B. Interestingly, 3, 5-diiodotyrosine is a putative diet iodine supplement with very good safety, indicating its unique advantage as a cancer chemoprevention agent.

### The somatic mutation inhibitory activity and structure-activity relationship of 3, 5-diiodotyrosine

To further confirm whether 3, 5-diiodotyrosine could inhibit the somatic mutation-driver function of APOBEC3B, we tried to use APOBEC3B overexpressed *E. coli* and performed bacterial resequencing assay to determine whether 3,5-diiodotyrosine could reduce the number of specific single-nucleotide polymorphisms (SNPs), which mainly including single nucleotide substitution. As shown in figure 2H, after 3, 5-diiodotyrosine treatment, the C>T transversion driven by APOBEC3B in *E. coli* genome was significant reduced, suggesting 3, 5-diiodotyrosine could effectively inhibit the cytosine deaminase activity and attenuate the DNA mutation driven by APOBEC3B. In addition, 3, 5-diiodotyrosine could not inhibit the proliferation of KYSE70 cells (online supplemental figure S6A), but could down-regulated the expression of APOBEC3B (online supplemental figure S6B). Taken together, these results suggested that 3,

5-diiodotyrosine could prevent the somatic mutation through inhibiting the activity and the expression of APOBEC3B.

Next, the detailed interactions between 3, 5-diiodotyrosine and APOBEC3B were simulated. 3, 5-diiodotyrosine located at the catalytic site of APOBEC3B (figure 2I). Molecule docking showed that the affinity of 3, 5-diiodotyrosine to APOBEC3B was very strong (S value  $-9.08$ ). 3, 5-diiodotyrosine interacted with the residues of R211, R274, W277, and E241 in APOBEC3B, and formed a covalent bond with zinc ion (active site). We further obtained seven analogs after similarity searching and investigated the structure-activity relationship of 3, 5-diiodotyrosine. As shown in figure 2J, when one iodine (I) atom at  $R_1$  or  $R_2$  was replaced, the bioactivity of 3, 5-diiodotyrosine was greatly reduced. When both of the two iodine (I) atoms were replaced, the bioactivity was totally impaired. While the amino group ( $\text{NH}_2$ ) at  $R_3$  site or carboxyl at  $R_4$  site were replaced, the inhibitory activity was also greatly reduced. These results suggested that the structure of this natural product 3, 5-diiodotyrosine was optimal to inhibit the enzyme activity of APOBEC3B, especially the two iodine atoms were very important.

### The chemoprevention effect of 3, 5-diiodotyrosine in 4-NQO-induced ESCC mouse model

To investigate the chemoprevention effect and mechanism, we chose the putative spontaneous ESCC mouse model induced by 4-nitroquinoline 1-oxide (4-NQO) as the mouse model. Results in online supplemental figure S7A-D showed that during the process of induction, the water and food intake, body weight and activity status of mice in 4-NQO-induced group were worse than those in non-induced group. The H&E staining results confirmed that esophagus tissues at week 28 were considered as high-grade intraepithelial neoplasia, which indicated that the ESCC mouse model was successfully established (online supplemental figure S7E). Here, it was worth mentioning that there was no subtype of APOBEC3 in murine.<sup>38 39</sup> Therefore, the APOBEC3 expression was verified in esophagus tissues at different stages of 4-NQO-induced ESCC mice by using qRT-PCR assay. Result in online supplemental figure S7F showed that the APOBEC3 expression in induced mice was increased from week 20 and reached the highest level at week 28, which was much higher than that of naive mice at the same age. Furthermore, the protein level of APOBEC3 was highly expressed in esophagus tissues of 4-NQO-induced mouse (online supplemental figure S7G).

Next, 3, 5-diiodotyrosine was used to treat ESCC mice (*i.p.*) at a low dose (0.5mg/kg) and a high dose (2mg/kg), respectively (figure 3A). Results showed that the number and length of ESCC tumor tissue were significantly reduced compared with normal saline (NS) group (figure 3B). Both low and high dose of 3, 5-diiodotyrosine group could significantly prolong the overall survival of mice, and slow down the loss trend of body weight (figure 3C and online supplemental figure S8A). H&E

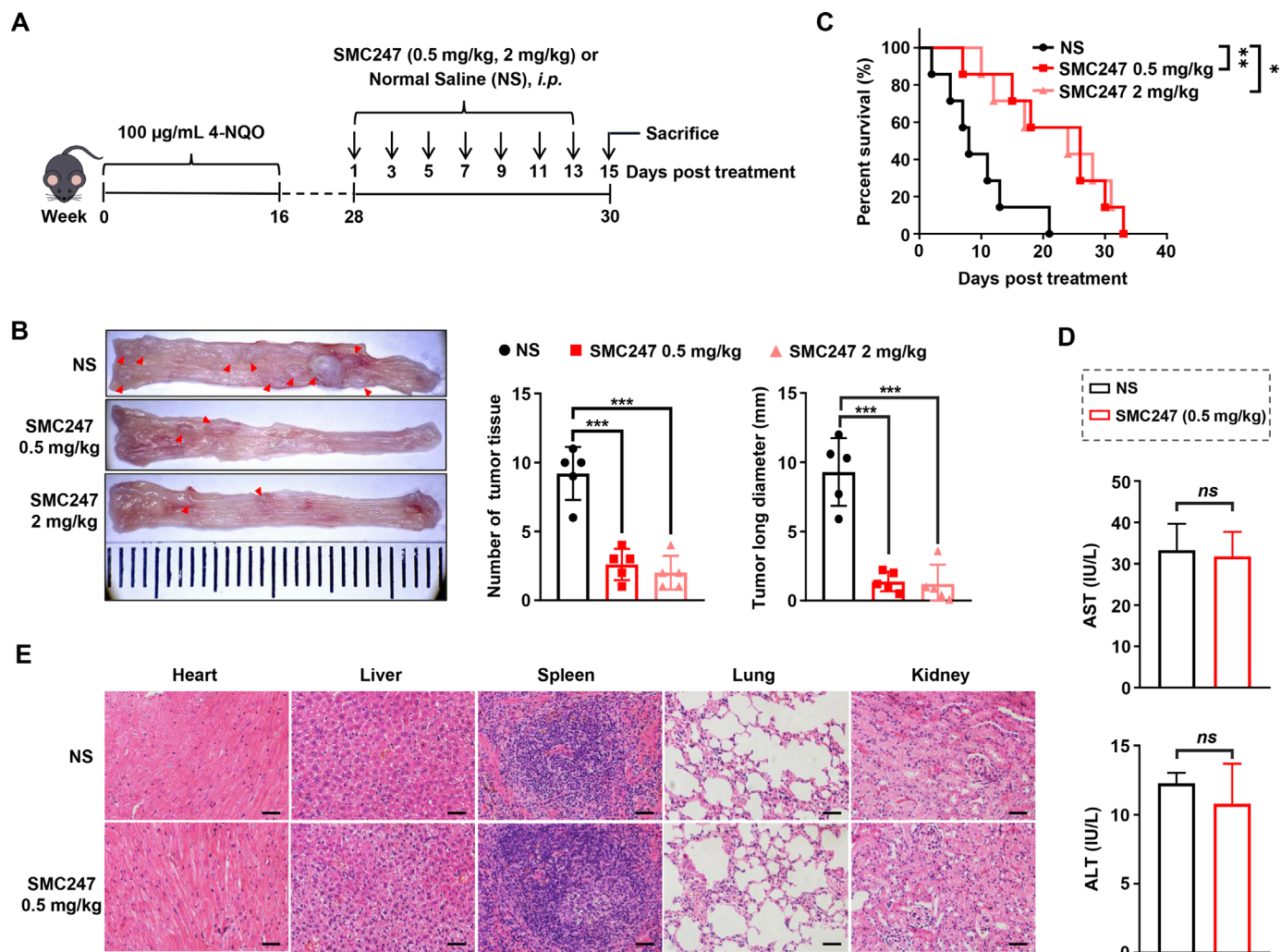


**Figure 3** The chemoprevention effects of 3, 5-diiodotyrosine in 4-NQO-induced ESCC mouse model. (A) Schematic illustration of the *in vivo* experiment. (B) Tissues appearance of the esophageal epithelium, number and long diameter of tumor tissues in mice treated by normal saline, 0.5 mg/kg or 2 mg/kg 3, 5-diiodotyrosine ( $n=5$ ,  $***p<0.001$ ). (C) Survival curve of mice ( $n=7$ ,  $*p<0.05$ ,  $**p<0.01$ ). (D) Analysis of hepatic damage by the level of AST and ALT in serum ( $n=5$ ). *ns*, no statistical difference. (E) The H&E staining of mice organs after treatment (scale bars: 100  $\mu$ m for heart, liver, lung and kidney, 50  $\mu$ m for spleen). The data are presented as mean  $\pm$  SEM. ALT, alanine aminotransferase; AST, aspartate transaminase.

results in online supplemental figure S8B showed that the epithelial layer of esophagus was thickened, the cell polarity of mucosal layer was disappeared, and the nuclei became larger and hyperchromatic in NS group, but all of these symptoms resolved after 3, 5-diiodotyrosine treatment.

To confirm the safety of 3, 5-diiodotyrosine, experiments were conducted both *in vitro* and *in vivo*. Serum samples of each mouse in NS group and 0.5 mg/kg 3, 5-diiodotyrosine group were collected and used to test AST and ALT indexes representing hepatic damage. Results suggested that there were no significant differences (figure 3D). The H&E staining assay for the main viscera of each group showed that there were no obvious toxic effects (figure 3E). Subsequently, the effect of 3, 5-diiodotyrosine on three non-tumoral cell lines was detected by MTT assay. As shown in online supplemental figure S9A-C, 3, 5-diiodotyrosine did not affect the viability of these cells. Furthermore, naive female C57BL/6J mice

(7 weeks) were randomly divided, and were *i.p.* injected every 2 days for 2 weeks with 200  $\mu$ L normal saline and different dosages of 3, 5-diiodotyrosine. After treatment, fresh anticoagulant whole blood was collected quickly for blood routine analysis and the serum was obtained for blood biochemistry analysis (online supplemental figure S10A). Results showed that blood routine indexes (white cell count (WBC), hemoglobin (HGB), platelet (PLT) and red blood cells (RBC)), and blood biochemical (AST and ALT) indexes of each group were within the normal range, and has no significant differences (online supplemental figure S10B-G). These results suggested that low dose of 0.5 mg/kg 3, 5-diiodotyrosine was enough to effectively inhibit the progression of ESCC, with no obvious toxic effects.

### Effect of 3, 5-diiodotyrosine treatment on single base mutations in 4-NQO-induced ESCC mice

Furthermore, we performed whole exome sequencing to verify whether 3, 5-diiodotyrosine could inhibit the deaminase function of APOBEC3 *in vivo*. As shown in figure 4A, after 3, 5-diiodotyrosine treatment, the number of mutations at exome levels was significantly reduced compared with NS group. Among the six types of single base mutations, mutation counts of C>T and C>G were reduced in 3, 5-diiodotyrosine treatment group, which include CT motifs preferred by APOBEC3 (figure 4B–D). Interestingly, we also discovered that there was a reduction of C>A mutation type in mice. More importantly, after 3, 5-diiodotyrosine treatment, the contribution of APOBEC activity related signatures (SBS2 and SBS13) was weakened, further suggesting that 3, 5-diiodotyrosine could inhibit the enzyme activity of APOBEC3 (figure 4E). Correlation analysis also showed that the correlation of signature SBS2 and SBS13 resulted by APOBEC3 was significantly weakened (figure 4F).

Further, we investigated the significant mutant genes (SMGs) and identified the genes with decreased mutation in 3, 5-diiodotyrosine treatment group (figure 4G). Subsequently, we analyzed the association of these genes in the progression of ESCC. Most of these genes are tumor suppressor genes in ESCC and their tumor suppressive ability will be impaired or even be reversed once mutated.<sup>40</sup> Missense mutation of many genes, such as TTN (also named cardiomyopathy, dilated 1G (CMD1G)) was positively associated with the poor progression-free survival of ESCC patients.<sup>41</sup> Zinc finger homeobox 4 (ZFHX4) could reduce the migration and invasion ability of ESCC cells, but mutation of ZFHX4 was closely associated with poor prognosis of ESCC patients.<sup>42</sup> Other genes, such as FAT atypical cadherin 3 (Fat3), Dynein axonemal heavy chain 5 (DNAH5) and Netrin receptor DCC (DCC) were recurrently mutation genes in ESCC.<sup>43</sup> These results suggested that 3, 5-diiodotyrosine could inhibit the enzyme activity of APOBEC3 and reduce the mutation burden driven by APOBEC3 *in vivo*, and thus achieved good chemoprevention effects on ESCC.

### The synergistic chemoprevention effect of 3, 5-diiodotyrosine combined with PD-1/PD-L1 blockade on 4-NQO-induced ESCC mouse model

Aside from the accumulation of somatic mutation, the immune microenvironment also plays important role during cancer occurrence. Therefore, we analyzed the correlation between the expression of APOBEC3B and the infiltration of CD8<sup>+</sup> T cell. Results shown in figure 5A suggested that APOBEC3B expression was negatively correlated with CD8<sup>+</sup> T infiltration. High expression of APOBEC3B was found to be significantly associated with decreased expression of CD8A and CD8B (figure 5B). Furthermore, high expression level of APOBEC3B was also significantly associated with reduced T cell effectors IFNG, GZMH and GZMK, which were main factors for tumor-killing (figure 5C,D). Surprisingly, we found that

3, 5-diiodotyrosine could up-regulate the expression of PD-L1 at the concentration of 10 μM and 100 μM (online supplemental figure S11A).

Based on these results, we attempted to combine 3, 5-diiodotyrosine with a PD-1/PD-L1 inhibitor to treat ESCC mice (figure 5E). Before that, we analyzed that the PD-L1 expression in esophagus tissues of induced mouse were increased continuously from week 20 to week 28, which indicated that the microenvironment of the precancerous lesion getting immune-suppressive during cancer occurrence aside from somatic mutation accumulation (online supplemental figure S11B). Results in figure 5F showed that the number and length of ESCC tumor tissues were significantly reduced in 3, 5-diiodotyrosine or OPBP-1 group. The synergistic cancer prevention effects were observed in 3, 5-diiodotyrosine and OPBP-1 combination group. Furthermore, the proportions of IFN-γ<sup>+</sup>CD8<sup>+</sup> T cells in both spleen and lymph node were increased in 3, 5-diiodotyrosine or OPBP-1 group, and had synergistic enhancement effect in combination group (figure 5G). Through anatomical observation and H&E staining assay for esophagus tissues, the epithelial layer of esophagus was thickened, the cell polarity of mucosal layer was disappeared, and the nuclei became larger and hyperchromatic in NS group. In OPBP-1 alone group, esophageal tissues still had a certain phenomenon of thickening. In 3, 5-diiodotyrosine alone and combination intervention group, these symptoms were effectively alleviated (figure 5H). Moreover, survival experiment was conducted. Interestingly, 0.5 mg/kg OPBP-1 did not significantly prolong the survival of mice, and the effect was much weaker than that of 0.5 mg/kg 3, 5-diiodotyrosine group, but the survival times of 60% mice in combination group was more than 50 days, which was significantly higher than that of 3, 5-diiodotyrosine monotherapy (figure 5I). These results showed that the cancer prevention effects of 3, 5-diiodotyrosine could be improved through combination with PD-1/PD-L1 blockade.

### 3, 5-diiodotyrosine combined with PD-1/PD-L1 blockade elicits synergistic cancer prevention effects on AOM/DSS-induced colon cancer mouse model

In order to further confirm the cancer prevention effect of 3, 5-diiodotyrosine combined with PD-1/PD-L1 blockade, we examined the effect of 3, 5-diiodotyrosine on PD-L1 expression in colon cancer cell RKO. Consistent with the results in ESCC, 3, 5-diiodotyrosine could up-regulate the expression of PD-L1 (online supplemental figure S12).

Subsequently, we established the AOM/DSS-induced colon cancer mouse model, which could simulate the whole process from normal mucosa, precancerous lesions to tumor formation (figure 6A). The pathological characteristics were similar to human colon cancer, and could reflect the development pattern from colitis to tumor in human. First, we analyzed the APOBEC3 expression and PD-L1 expression in colon tissues at different stages of AOM/DSS-induced colon cancer mouse using GEO

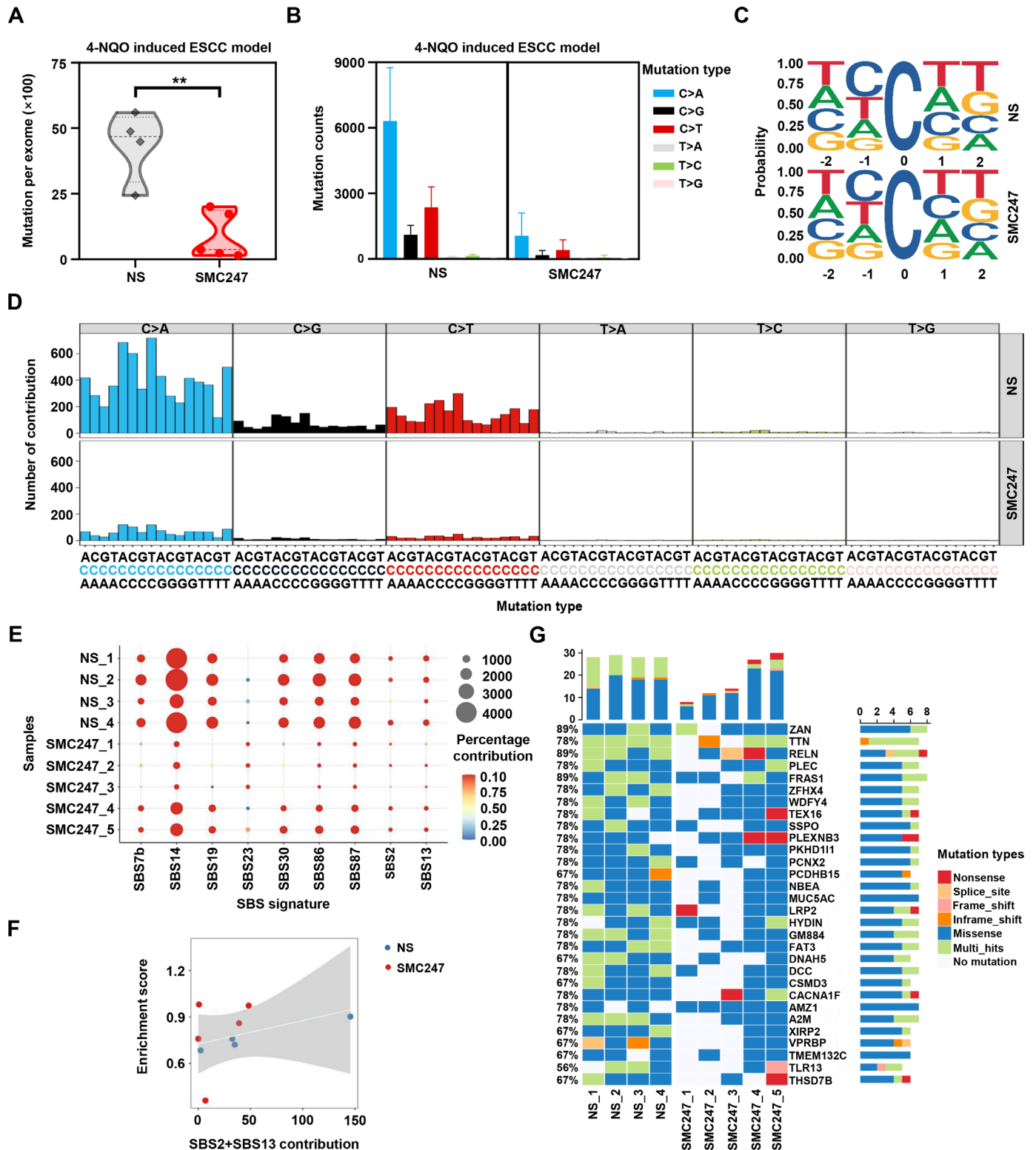


**Figure 4** Effect of 3, 5-diiodotyrosine on single base substitution mutations in 4-NQO-induced ESCC mice based on whole exome sequencing. The 4-NQO-induced mice were treated (*i.p.*) with NS and 0.5 mg/kg 3, 5-diiodotyrosine every 2 days for 2 weeks. (A) Total mutations per exome in NS group (n=4) and 3, 5-diiodotyrosine group (n=5). Mean was shown by horizontal line,  $**p < 0.01$  by one-tailed Student's *t*-test. (B) The mutation counts of six kinds of single base substitution mutation. (C) Sequence logos for all C mutations in tumors. (D) Trinucleotide mutation profiles of all base substitutions in each group. (E) The relative contribution significantly changed cosmic SBS signatures (Wilcox test,  $p < 0.1$ ). (F) The correlation between contribution of APOBEC-related mutation signatures (SBS2 and SBS13) and APOBEC enrichment score. Spearman's correlation coefficient  $R = 0.36$ . (G) The top 30 significant mutant genes after NS or 3, 5-diiodotyrosine treatment. The white squares represented genes without mutation in corresponding samples.

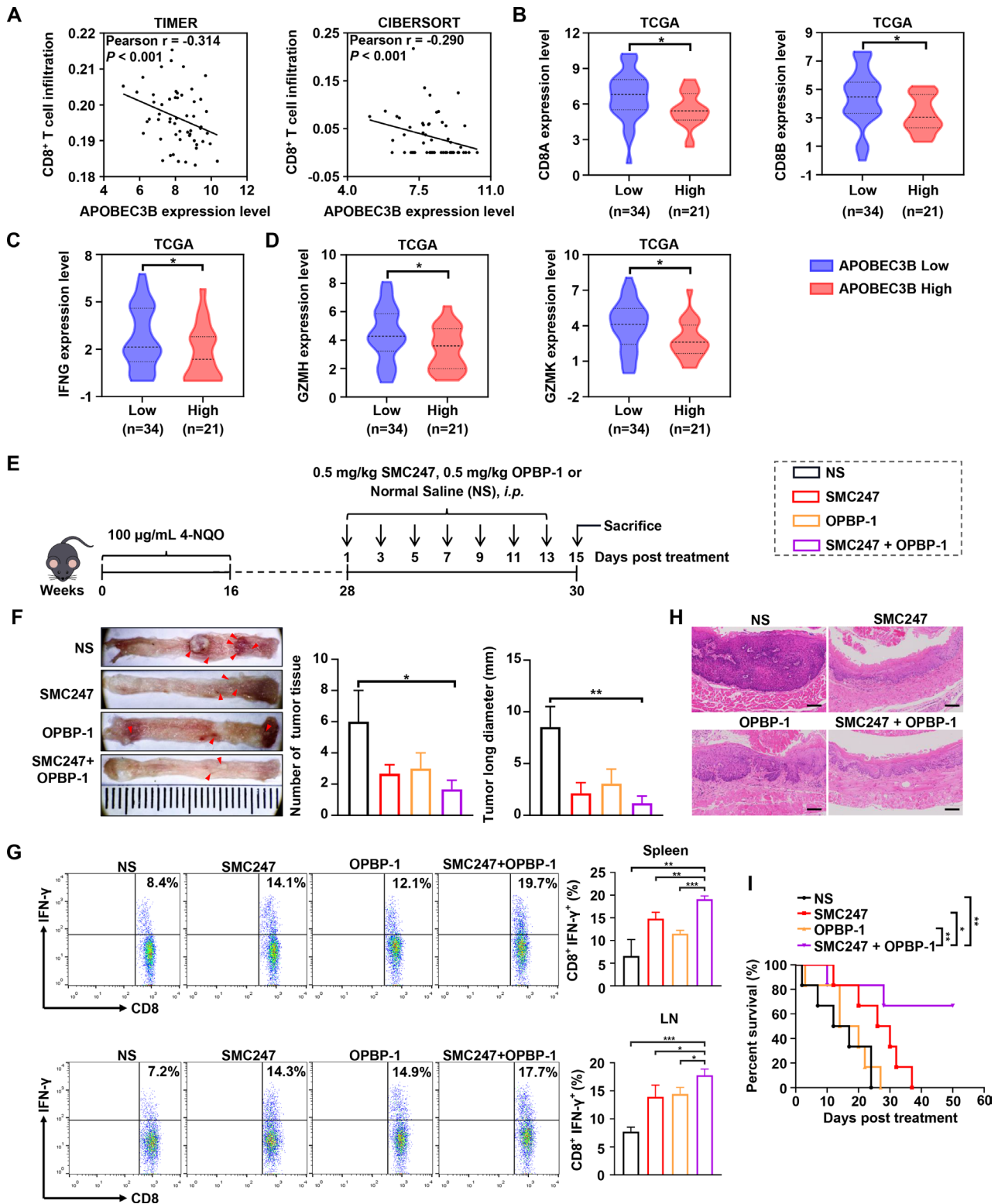


**Figure 5** The synergistic chemoprevention effects of 3, 5-diiodotyrosine combined with PD-1/PD-L1 blockade on 4-NQO induced ESCC mouse model. (A) CD8 $^+$  T cell infiltration was assessed based on mRNA expression level of APOBEC3B with TIMER and CIBERSORT.  $P$  values were determined by Wilcoxon test. (B–D) The mRNA expression of CD8A, CD8B and T effector genes were quantitatively analyzed between APOBEC3B low ( $n=34$ ) and APOBEC3B high ( $n=21$ ) expression status.  $*p < 0.05$  by one-tailed Student's  $t$ -test. (E) Schematic illustration of the *in vivo* experiment. ESCC mice were *i.p.* injected with NS, 0.5 mg/kg 3, 5-diiodotyrosine, 0.5 mg/kg OPBP-1 or 3, 5-diiodotyrosine combined with OPBP-1 every 2 days for 2 weeks. (F) Tissues appearance of the esophageal epithelium, number and long diameter of tumor tissues in mice ( $n=3$ ). (G) The proportion of IFN- $\gamma$  $^+$ CD8 $^+$  T cells in spleen and lymph node cells was detected by intracellular cytokine staining ( $n=3$ ,  $*p < 0.05$ ,  $**p < 0.01$ ,  $***p < 0.001$ ). The data are presented as mean  $\pm$  SEM. (H) Histopathological assessment of esophagus tissues in each group was determined by H&E staining assay (scale bars: 100  $\mu$ m). (I) Survival curve of mice ( $n=6$ ).

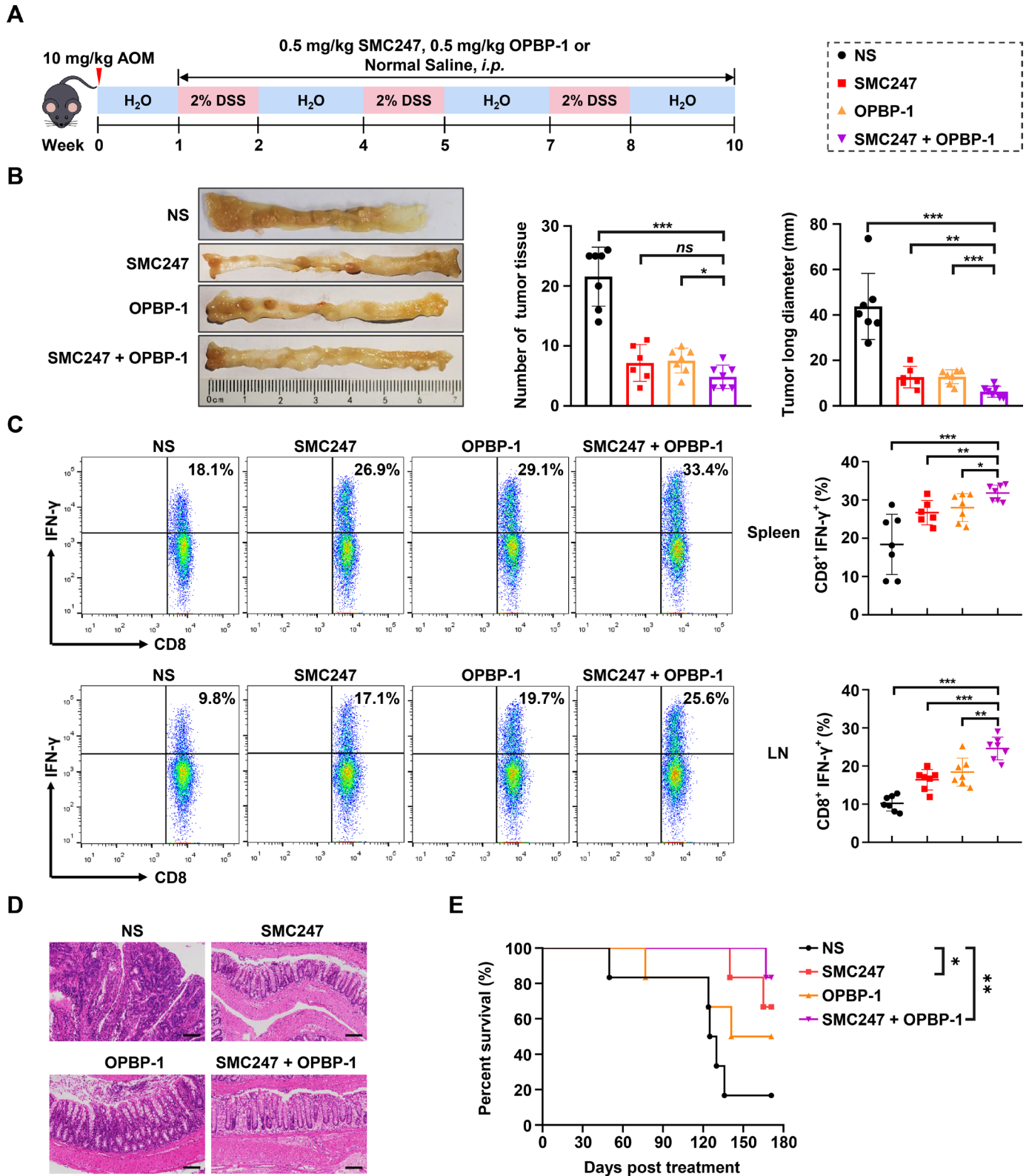


**Figure 6** The synergistic chemoprevention effects of 3, 5-diiodotyrosine combined with PD-1/PD-L1 blockade on AOM/DSS induced colon cancer mouse model. (A) Schematic illustration of the *in vivo* experiment. The mice were *i.p.* injected with NS, 0.5 mg/kg 3, 5-diiodotyrosine, 0.5 mg/kg OPBP-1 or 3, 5-diiodotyrosine combined with OPBP-1 every 2 days for 9 weeks (three rounds of DSS induction). (B) Tissues appearance of the colon epithelium, number and long diameter of tumor tissues in mice. *ns*, no statistical difference. (C) The proportion of IFN- $\gamma$ <sup>+</sup>CD8<sup>+</sup> T cells in spleen and lymph node cells was detected by intracellular cytokine staining ( $n=6$  or  $7$ ,  $*p<0.05$ ,  $**p<0.01$ ,  $***p<0.001$ ). The data are presented as mean $\pm$ SEM. (D) Histopathological assessment of colon tissues in each group after treatment was determined by H&E staining assay (scale bars: 100  $\mu$ m). (E) Survival curve of mice ( $n=6$ ). DSS, dextran sulfate sodium.

dataset, and found that the mRNA expression levels of APOBEC3 and PD-L1 in colon tissues increased continuously with the colon cancer occurrence (online supplemental figure S13A, C). Then we confirmed the expression profile of APOBEC3 and PD-L1 in colon tissues in AOM/DSS-induced mouse model (online supplemental figure S13B, D). In AOM/DSS-induced mouse model, both 3, 5-diiodotyrosine group or OPBP-1 group could significantly slow down the trend of body weight loss, decreased the disease activity index (DAI) of mice, and significantly reduced the number and size of tumors in colonic epithelial tissues without changing the length of colon basically. The detailed assessment standard of DAI was shown in online supplemental table S6. All these effects were more pronounced in 3, 5-diiodotyrosine and OPBP-1 combination group (online supplemental figure S14A-C, [figure 6B](#)). Moreover, the proportions of IFN- $\gamma^+$ CD8 $^+$  T cells in both spleen and lymph node were increased in 3, 5-diiodotyrosine or OPBP-1 group, especially in combination group ([figure 6C](#)), with no obvious toxic effects (online supplemental figure S14D, E).

Through the anatomical observation and H&E staining assay of colon tissue, results showed that the epithelium of colon tissues was eroded and thickened, epithelial cells were destroyed, crypts were destroyed, goblet cells were lost, and a large number of tumor cells appeared in NS group ([figure 6D](#)). After 3, 5-diiodotyrosine or/and OPBP-1 intervention, these symptoms were effectively alleviated. In the OPBP-1 alone group, the colonic epithelium showed atypical hyperplasia and inflammatory cell infiltration. In the 3, 5-diiodotyrosine alone group, the colonic mucosa was intact and the glandular cells were basically arranged in order. In combination group, it could be observed that the villi in the colonic epithelial tissue were orderly and complete. Furthermore, we observed that OPBP-1 could prolong the survival of mice to some extent, and the effect was much weaker than that of 3, 5-diiodotyrosine group, but more than 80% of mice survived for than 170 days in combination group, with a more significant effect ([figure 6E](#)). Collectively, the above results proved that 3, 5-diiodotyrosine could prevent the development and progression of tumor by inhibiting APOBEC3B mutation-driving activity, and showed synergistic effects with PD-1/PD-L1 blockade.

### 3, 5-diiodotyrosine promotes the proliferation and function of CD8 $^+$ T cells via IL-15 in tumor microenvironment

In 4-NQO-induced ESCC and AOM/DSS-induced colon cancer mouse model described above, the tumor infiltration and function of CD8 $^+$  T cells was significantly increased in the 3, 5-diiodotyrosine group. Thus, we sought to investigate the mechanism involved. First, human PBMCs were treated with 10  $\mu$ M 3, 5-diiodotyrosine for 3 days, result suggested that 3, 5-diiodotyrosine did not directly affect the function of CD8 $^+$  T cells in the absence of tumor cells (online supplemental figure S15A). Then, activated PBMCs were cocultured with KYSE70 cells treated with or without 10  $\mu$ M 3, 5-diiodotyrosine, results showed that

3, 5-diiodotyrosine promoted the proliferation of CD8 $^+$  T cells and proportion of IFN- $\gamma^+$ CD8 $^+$  T cells (online supplemental figure S15B, C). To further confirm this promotion effect is caused by direct interaction between T cells and tumor cells, or cytokines secreted by tumor cells after 3, 5-diiodotyrosine treatment, the supernatants of KYSE70 cells pretreated with or without 10  $\mu$ M 3, 5-diiodotyrosine for 48 hours were collected and cultured with human PBMCs for 3 days. Results showed that the promotion effect on CD8 $^+$  T cells in the 3, 5-diiodotyrosine group was still existed ([figure 7A,B](#)).

The increased count of CD8 $^+$  T cells in tumor may be due to the recruitment or proliferation of CD8 $^+$  T cell. So, the chemotaxis of CD8 $^+$  T cells were performed. Results showed that 3, 5-diiodotyrosine could not promote the migration of CD8 $^+$  T cells (online supplemental figure S15D). Therefore, we think that some secretory proteins associated with T cell proliferation played a vital role. Subsequently, transcriptome sequencing on KYSE70-vehicle cells and KYSE70 cells treated by 10  $\mu$ M 3, 5-diiodotyrosine for 48 hours were performed to find the candidate secretory protein. Through analyzing the upregulated secretory genes that affecting T cell function, results showed that IL-7 and IL-15 were significantly upregulated in the 3, 5-diiodotyrosine group ([figure 7C](#)). After qRT-PCR verification, the changes of IL-7 and IL-15 expression levels in two groups were consistent with the above sequencing results ([figure 7D](#)). ELISA assay was further performed to measure the secretion levels of IL-7 and IL-15, results showed that the secretion level of IL-7 and IL-15 in the supernatants of KYSE70 treated with 10  $\mu$ M 3, 5-diiodotyrosine was significantly greater than in vehicle supernatants ([figure 7E](#)), but the IL-7 expression level was too low.

To further confirm the key role of IL-15, IL-15 neutralizing antibody was added into above coculture system. Interestingly, IL-15 neutralizing antibody could neutralize the function of 3, 5-diiodotyrosine on CD8 $^+$  T cells in terms of the proliferation and function of CD8 $^+$  T cells ([figure 7F,G](#)). These results suggested that 3, 5-diiodotyrosine could enhance the tumor infiltration and function of CD8 $^+$  T cells by stimulating tumor cells to secrete IL-15.

In summary, normal epithelial cells, in certain cases, would gradually develop into the precancerous lesions during the transformation, and eventually develop into invasive carcinoma without intervention. We observed that the expression of APOBEC3B was elevated and functioned as mutation driver during the development and progression of cancer ([figure 8](#)). By screening the natural product library, we discovered for the first time that 3, 5-diiodotyrosine from kelp could serve as a promising candidate for the chemoprevention of cancer through inhibiting the effect of cytosine deamination on ssDNA and genomic instability caused by APOBEC3B, and enhancing the tumor infiltration and function of CD8 $^+$  T cells via IL-15 in tumor environment. Moreover, 3, 5-diiodotyrosine could achieve synergistic

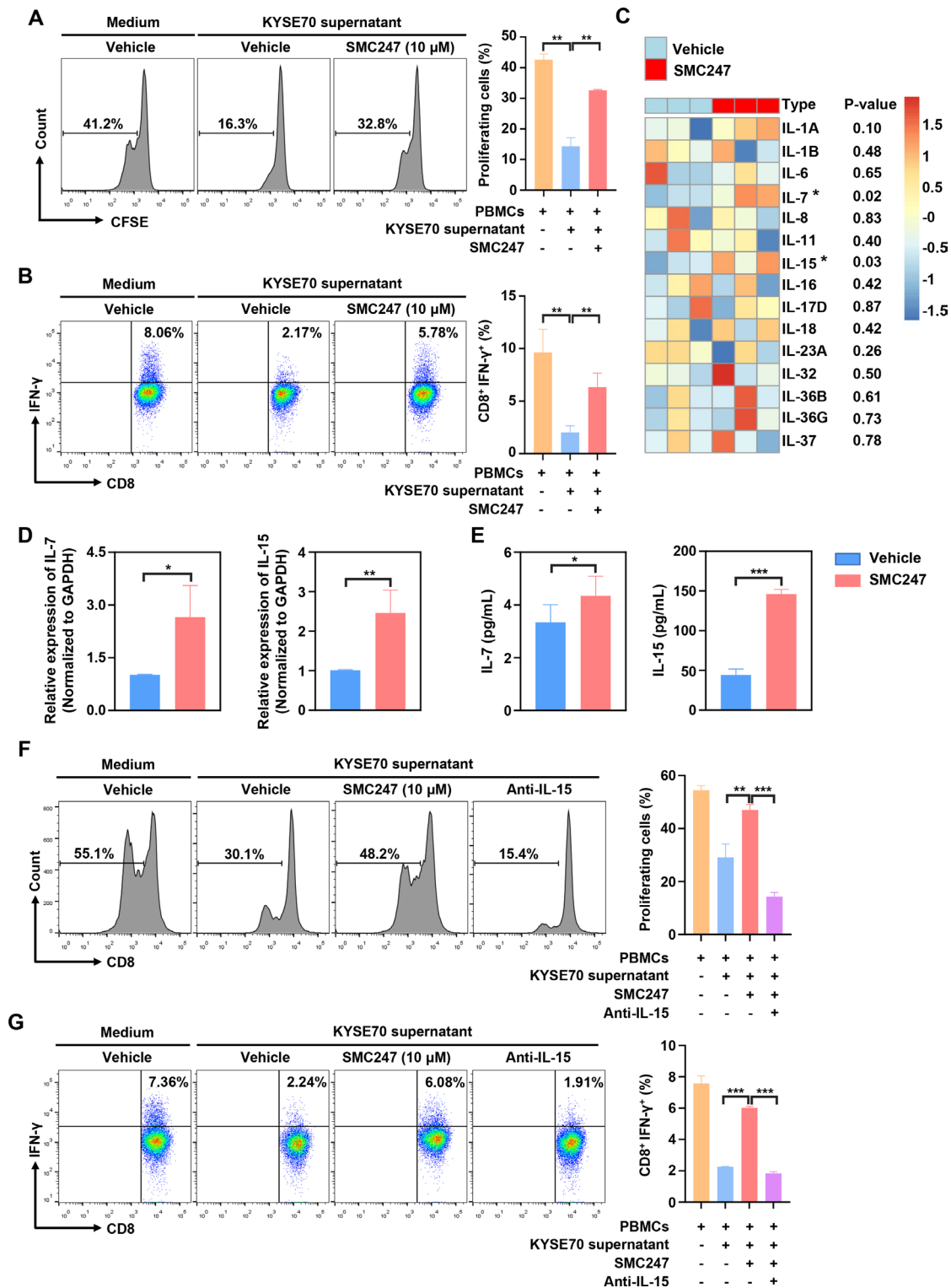


**Figure 7** 3, 5-diiodotyrosine promotes the proliferation and function of CD8<sup>+</sup> T cells via IL-15 in tumor microenvironment. (A, B) PBMCs from human volunteers were isolated and stained with 0.2 μM CFSE. Then, PBMCs were activated with 100 units IL-2, 1 μg/mL anti-CD3, and 1 μg/mL anti-CD28 stimulatory antibodies, and cultured in the supernatant of KYSE70 cells pretreated with or without 10 μM 3, 5-diiodotyrosine. After 3 days, the proliferation of CD8<sup>+</sup> T cells and proportion of IFN-γ<sup>+</sup>CD8<sup>+</sup> T cells were analyzed by flow cytometry. (C) KYSE70 cells with and without 3, 5-diiodotyrosine treatment for 48 hours were analyzed by whole transcriptome sequencing. The upregulated inflammatory factors in 3, 5-diiodotyrosine treatment group were analyzed. (D, E) The mRNA and protein expression levels of IL-7 and IL-15 in vehicle group and 3, 5-diiodotyrosine treated KYSE70 cells group were further verified by qRT-PCR and ELISA. Mean±SD were shown for triplicate reactions normalized to GAPDH. (F) The proliferation of CD8<sup>+</sup> T cells and proportion of IFN-γ<sup>+</sup>CD8<sup>+</sup> T cells in PBMCs treated with IL-15 neutralizing antibody were analyzed by flow cytometry. Data and representative figures are representative of at least three independent experiments, \**p*<0.05, \*\**p*<0.01, \*\*\**p*<0.001 by one-tailed Student's *t*-test.



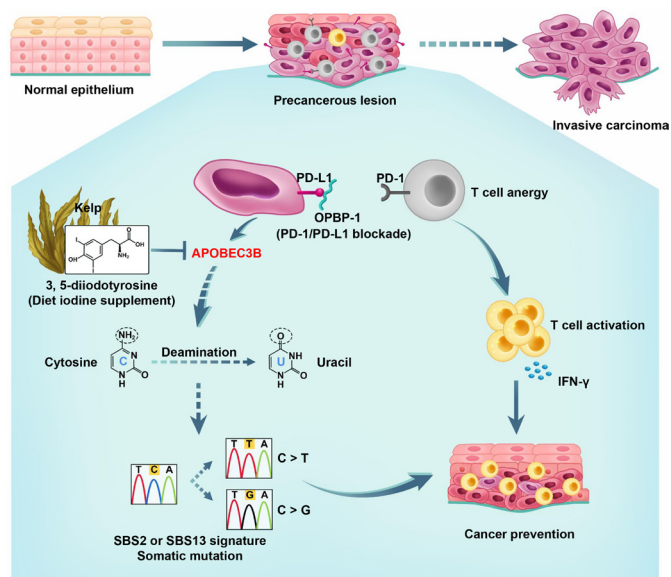


**Figure 8** Schematic illustration of cancer chemoprevention mechanism of 3, 5-diiodotyrosine combined with PD-1/PD-L1 blockade.

chemoprevention effects when combined with PD-1/PD-L1 blockade.

## DISCUSSION

More and more patients developed early-stage carcinoma or precancerous lesions in areas with high tumor incidence.<sup>44–45</sup> Unfortunately, because of lacking promising drug targets, there are no effective prevention and therapeutic drugs for these cases up to now. Therefore, it is urgent to develop potential chemoprevention agents to prevent the occurrence and development of cancer.

The next-generation sequencing studies indicated that there were multiple mutations in human cancers.<sup>46</sup> However, the dominant endogenous mutation driver is still unclear. Some studies have shown that APOBEC3B, a member of APOBEC family, is a major source of mutation driver in a variety of cancer types.<sup>47–48</sup> Here, we found that SBS characteristics associated with SBS2 and 13 signatures resulted from APOBEC3B were widespread in pan-cancer based on TCGA dataset. We also found that APOBEC3B was overexpressed in many cancers, its high expression was correlated with poor prognosis in cancer patients. Moreover, it was reported that APOBEC3B could lead to chromatin variation, DNA damage, and genome instability through its strong nucleic acid editing ability, and further promoted the occurrence and progression of cancer.<sup>49</sup> Thus, it will be of great clinical significance to study the mutation-driven mechanism of APOBEC3B and discover its inhibitors for the cancer chemoprevention. Although oligonucleotide drugs targeting APOBEC3B have been reported, APOBEC3B is mainly localized in the nucleoplasm and has the good stability *in vivo*. So, the development of small molecule inhibitors will be more valuable.

Natural products which are mainly derived from plants, animals and microorganisms, have a wide range of biological activities and low toxicity, which make them as ideal cancer chemoprevention agent candidates.<sup>50–51</sup>

Up to now, there are no natural compound inhibitors of APOBEC3B have been reported yet. In this study, we found that 3, 5-diiodotyrosine was located in the active pocket of APOBEC3B and effectively inhibited deaminase function of APOBEC3B. Besides, results of bacterial resequencing and whole exome sequencing showed that 3, 5-diiodotyrosine could reduce clusters of mutations and C>T mutation type driven by APOBEC3B. Furthermore, the mutations of genes TTN, ZFH4, and FAT3 were prevented after 3, 5-diiodotyrosine treatment, most of them were tumor suppressor genes and with missense mutations frequently occurring in cancer.<sup>40–42</sup> All these results suggested that 3, 5-diiodotyrosine slowed down the development of cancer by reducing the somatic mutation accumulation caused by APOBEC3B. More importantly, 3, 5-diiodotyrosine has been reported as a major component from the extract of kelp and be used as the resource of dietary iodine with very good safety.<sup>52</sup> Nelson *et al* suggested that long-term intake of iodine-rich seaweed and kelp could inhibit the development of tumors, but the mechanisms remain unclear.<sup>53–55</sup> Therefore, our studies not only revealed the possible chemoprevention mechanism of kelp, but also proposed the novel aspect to the reposition of 3, 5-diiodotyrosine. As 3, 5-diiodotyrosine is also involved in the biosynthesis of T4 or T3 thyroid hormones, the evaluation of APOBEC3B expression and function in the thyroid cancer cells (THCA) was also performed. We found that APOBEC3B expression level was much higher in tumor tissues than in normal tissues in anaplastic thyroid cancer, and was correlated with poor prognosis of THCA (online supplemental figure S16A–D). Furthermore, there was no significant difference in the expression of thyroid-stimulating hormone, free triiodothyronine (fT3) and free thyroxine (fT4) between 3, 5-diiodotyrosine group and NS group (online supplemental figure S17A–D).

The immune microenvironment also plays important role during cancer occurrence. Aydın *et al* reported that the expression levels of immune checkpoints such as PD-1 and PD-L1 continuously increased in precancerous lesions that developed to malignancies.<sup>56–57</sup> Mascaux *et al* reported that immune escape through immune checkpoint was found in early lung squamous carcinogenesis.<sup>58</sup> Wang *et al* reported that anti-PD-1 treatment could prevent the progression of oral premalignant lesions.<sup>59</sup> In the current study, we found that PD-L1 expression in esophagus tissues of 4-NQO-induced ESCC and in colon tissues of AOM/DSS-induced colon cancer mouse models were increased continuously during the progression of precancerous lesions. All these results indicated that the immune-suppressive immune microenvironment of the precancerous lesion during cancer occurrence also played an important role aside from the accumulation of somatic mutation. Here, we found that the high



expression of APOBEC3B was associated with reduced CD8 T cell genes (CD8A, CD8B) and T cell effectors (IFNG, GZMH and GZMK) in ESCC patients, this result was consistent with the reports in hepatocellular carcinoma and gastric cancer.<sup>19 48</sup> 3, 5-diiodotyrosine could significantly upregulated the expression of PD-L1 in tumor cells, which suggested that 3, 5-diiodotyrosine may be more effective in combination with inhibitors of immune checkpoint PD-L1.

Immune checkpoint blockade therapy has made breakthrough in clinical, but immune-related adverse effects (irAEs) are still a challenge, one of the most common toxicities is ICIs-associated colitis.<sup>60 61</sup> Furthermore, fatal toxic events most often occurred in the early stages after treatment initiation. ESMO Clinical Practice Guidelines recommend that the high-dose systemic corticosteroids could be used to treat colitis induced by ICIs at the initial stage,<sup>62</sup> but this will also bring more life-threatening complications, such as serious infection, thromboembolism, sleep disturbances, reduced bone mineral density and so on.<sup>63</sup> Alexander *et al* team used oral beclomethasone dipropionate to treat mild to moderate colitis induced by ICIs, with fewer side effects.<sup>64</sup> In addition, ongoing studies are evaluating the immunosuppression effect on antitumor efficacy. In colon cancer mouse model induced by AOM/DSS, the enteritis phenomenon was significantly relieved in mice of 3, 5-diiodotyrosine treatment group and 3, 5-diiodotyrosine combined with PD-1/PD-L1 blockade, which suggested that 3, 5-diiodotyrosine may be a promising candidate for colitis. Of course, more tumor models are needed to confirm this effect. Overall, we think that 3, 5-diiodotyrosine could effectively prevent the further deterioration of precancerous tissues by inhibiting the deaminase activity of APOBEC3B, reducing colitis and increasing the infiltration and function of IFN- $\gamma$ CD8<sup>+</sup> T cells. Therefore, 3, 5-diiodotyrosine combined with PD-1/PD-L1 blockade could also exert good synergistic cancer prevention effects and significantly prolonged the survival of mice. All results suggested that 3, 5-diiodotyrosine could not only prevent the occurrence of cancer, but also reduce the enteritis caused by current clinical treatment therapy such as ICIs. So, 3, 5-diiodotyrosine will have better and broader clinical perspectives combined with PD-1/PD-L1 blockade.

Aside from the accumulation of somatic mutation and the immunosuppressive microenvironment, there are some other carcinogenic factors, such as ROS production, side effects caused by chemotherapy drugs, and UV light exposure.<sup>65 66</sup> Studies have shown that the thioredoxin (TXN) and glutathione-related drugs could prevent the carcinogenesis caused by oxidative stress.<sup>67</sup> Dietary supplements such as vitamin B group and vitamin E played unique roles in cancer prevention, but the mechanism was still unclear.<sup>68</sup> Therefore, studying carcinogenic factors to discover novel chemoprevention drug targets and therapeutics may be the way forward.

## CONCLUSION

In conclusion, APOBEC3B was overexpressed in many cancers and acted as a somatic mutation driver. We first discovered that the natural product 3, 5-diiodotyrosine from kelp could be used as an ideal cancer chemoprevention agent by inhibiting the deaminase activity of APOBEC3B. Besides, 3, 5-diiodotyrosine could reduce the colitis and increase the infiltration and function of T lymphocytes via IL-15 in tumor microenvironment. 3, 5-diiodotyrosine combined with PD-1/PD-L1 blockade could elicit synergistic cancer prevention effects, indicating a novel strategy for both prevent the somatic mutation accumulation and the immune-suppressive microenvironment exacerbation. The good safety of 3, 5-diiodotyrosine makes it a very promising cancer chemoprevention agent.

## Author affiliations

<sup>1</sup>School of Life Sciences, Zhengzhou University, Zhengzhou, Henan, China

<sup>2</sup>School of Pharmaceutical Sciences (Shenzhen), Sun Yat-sen University - Shenzhen Campus, Shenzhen, Guangdong, China

<sup>3</sup>Henan Key Laboratory of Bioactive Macromolecules, Zhengzhou University, Zhengzhou, Henan, China

<sup>4</sup>Henan Key Laboratory of Immunology and Targeted Therapy, School of Laboratory Medicine, Xinxiang Medical University, Xinxiang, Henan, China

<sup>5</sup>International Joint Laboratory for Protein and Peptide Drugs of Henan Province, Zhengzhou University, Zhengzhou, Henan, China

**Contributors** YG and YW conceived and designed the experiments. CC performed most the experiments and wrote the first draft of the manuscript. XS helped to complete the analysis of the sequencing results. HN, YS, XC, XZ, GC, WS, LP, XZ, RS, WL, HW, WZ performed part of experiments, analyzed the data and revised the manuscript. JD helped to perform the virtual screening. WZ and YQ helped to analyze the data and revise the manuscript. All authors contributed to manuscript revision and approved the final version of this manuscript. YG and YW are responsible for the overall content as guarantor.

**Funding** This work was supported by the National Science Foundation of China (No. U20A20369, 81822043). 'Pearl River Talent Plan' Innovation and Entrepreneurship Team Project of Guangdong Province (2019ZT08Y464), and Shenzhen Science and Technology Program (KQTD20190929173853397).

**Competing interests** No, there are no competing interests.

**Patient consent for publication** Not applicable.

**Ethics approval** Experimental procedures and ethical consent were approved by the Ethics Committee Zhengzhou University (ZZU202003). Participants gave informed consent to participate in the study before taking part.

**Provenance and peer review** Not commissioned; externally peer reviewed.

**Data availability statement** All data relevant to the study are included in the article or uploaded as online supplemental information. Not applicable.

**Supplemental material** This content has been supplied by the author(s). It has not been vetted by BMJ Publishing Group Limited (BMJ) and may not have been peer-reviewed. Any opinions or recommendations discussed are solely those of the author(s) and are not endorsed by BMJ. BMJ disclaims all liability and responsibility arising from any reliance placed on the content. Where the content includes any translated material, BMJ does not warrant the accuracy and reliability of the translations (including but not limited to local regulations, clinical guidelines, terminology, drug names and drug dosages), and is not responsible for any error and/or omissions arising from translation and adaptation or otherwise.

**Open access** This is an open access article distributed in accordance with the Creative Commons Attribution Non Commercial (CC BY-NC 4.0) license, which permits others to distribute, remix, adapt, build upon this work non-commercially, and license their derivative works on different terms, provided the original work is properly cited, appropriate credit is given, any changes made indicated, and the use is non-commercial. See <http://creativecommons.org/licenses/by-nc/4.0/>.

## ORCID iD

Yanfeng Gao <http://orcid.org/0000-0001-5533-7100>

## REFERENCES

- Burns MB, Temiz NA, Harris RS. Evidence for APOBEC3B mutagenesis in multiple human cancers. *Nat Genet* 2013;45:977–83.
- Zou J, Wang C, Ma X, et al. APOBEC3B, a molecular driver of mutagenesis in human cancers. *Cell Biosci* 2017;7:29.
- Moody S, Senkin S, Islam SMA, et al. Mutational signatures in esophageal squamous cell carcinoma from eight countries with varying incidence. *Nat Genet* 2021;53:1553–63.
- Morita M, Kumashiro R, Kubo N, et al. Alcohol drinking, cigarette smoking, and the development of squamous cell carcinoma of the esophagus: epidemiology, clinical findings, and prevention. *Int J Clin Oncol* 2010;15:126–34.
- Hiatt RA, Brody JG. Environmental determinants of breast cancer. *Annu Rev Public Health* 2018;39:113–33.
- Wang S-M, Abnet CC, Qiao Y-L. What have we learned from linxian esophageal cancer etiological studies? *Thorac Cancer* 2019;10:1036–42.
- Marabotto E, Pellegatta G, Sheijani AD, et al. Prevention strategies for esophageal cancer—an expert review. *Cancers* 2021;13. doi:10.3390/cancers13092183. [Epub ahead of print: 01 05 2021].
- Wang J-B, Abnet CC, Fan J-H, et al. The randomized linxian dysplasia nutrition intervention trial after 26 years of follow-up: no effect of multivitamin supplementation on mortality. *JAMA Intern Med* 2013;173:1259–61.
- Limburg PJ, Wei W, Ahnen DJ, et al. Randomized, placebo-controlled, esophageal squamous cell cancer chemoprevention trial of selenomethionine and celecoxib. *Gastroenterology* 2005;129:863–73.
- Al-Sanea MM, Chilingaryan G, Abelyan N, et al. Combination of ligand and structure based virtual screening approaches for the discovery of potential PARP1 inhibitors. *PLoS One* 2022;17:e0272065.
- Jiang M, Jia K, Wang L, et al. Alterations of DNA damage response pathway: biomarker and therapeutic strategy for cancer immunotherapy. *Acta Pharm Sin B* 2021;11:2983–94.
- Brown JS, Sundar R, Lopez J. Combining DNA damaging therapeutics with immunotherapy: more haste, less speed. *Br J Cancer* 2018;118:312–24.
- Petljak M, Alexandrov LB, Brammeld JS, et al. Characterizing mutational signatures in human cancer cell lines reveals episodic APOBEC mutagenesis. *Cell* 2019;176:1282–94.
- Alexandrov LB, Nik-Zainal S, Wedge DC, et al. Signatures of mutational processes in human cancer. *Nature* 2013;500:415–21.
- Roberts SA, Lawrence MS, Klimczak LJ, et al. An APOBEC cytidine deaminase mutagenesis pattern is widespread in human cancers. *Nat Genet* 2013;45:970–6.
- Salter JD, Bennett RP, Smith HC. The APOBEC protein family: united by structure, divergent in function. *Trends Biochem Sci* 2016;41:578–94.
- Chen J, MacCarthy T. The preferred nucleotide contexts of the AID/APOBEC cytidine deaminases have differential effects when mutating retrotransposon and virus sequences compared to host genes. *PLoS Comput Biol* 2017;13:e1005471.
- Law EK, Siewewerts AM, LaPara K, et al. The DNA cytosine deaminase APOBEC3B promotes tamoxifen resistance in ER-positive breast cancer. *Sci Adv* 2016;2:e1601737.
- Wang D, Li X, Li J, et al. APOBEC3B interaction with PRC2 modulates microenvironment to promote HCC progression. *Gut* 2019;68:1846–57.
- Vieira VC, Leonard B, White EA, et al. Human papillomavirus E6 triggers upregulation of the antiviral and cancer genomic DNA deaminase APOBEC3B. *mBio* 2014;5. doi:10.1128/mBio.02234-14. [Epub ahead of print: 23 Dec 2014].
- Pak V, Heidecker G, Pathak VK, et al. The role of amino-terminal sequences in cellular localization and antiviral activity of APOBEC3B. *J Virol* 2011;85:8538–47.
- Shimizu A, Fujimori H, Minakawa Y, et al. Onset of deaminase APOBEC3B induction in response to DNA double-strand breaks. *Biochem Biophys Res* 2018;16:115–21.
- Bader SB, Ma TS, Simpson CJ, et al. Replication catastrophe induced by cyclic hypoxia leads to increased APOBEC3B activity. *Nucleic Acids Res* 2021;49:7492–506.
- Serebrenik AA, Argyris PP, Jarvis MC, et al. The DNA cytosine deaminase APOBEC3B is a molecular determinant of platinum responsiveness in clear cell ovarian cancer. *Clin Cancer Res* 2020;26:3397–407.
- Barzak FM, Harjes S, Kvach MV, et al. Selective inhibition of APOBEC3 enzymes by single-stranded DNAs containing 2'-deoxyzebularine. *Org Biomol Chem* 2019;17:9435–41.
- Kvach MV, Barzak FM, Harjes S, et al. Inhibiting APOBEC3 activity with single-stranded DNA containing 2'-deoxyzebularine analogues. *Biochemistry* 2019;58:391–400.
- Roberts TC, Langer R, Wood MJA. Advances in oligonucleotide drug delivery. *Nat Rev Drug Discov* 2020;19:673–94.
- Wang S, Du Z, Luo J, et al. Inhibition of heat shock protein 90 suppresses squamous carcinogenic progression in a mouse model of esophageal cancer. *J Cancer Res Clin Oncol* 2015;141:1405–16.
- Manicassamy S, Prasad PD, Swafford D. Mouse models of colitis-associated colon cancer. *Methods Mol Biol* 2021;2224:133–46.
- Li W, Zhu X, Zhou X, et al. An orally available PD-1/PD-L1 blocking peptide OPBP-1-loaded trimethyl chitosan hydrogel for cancer immunotherapy. *J Control Release* 2021;334:376–88.
- Alexandrov LB, Kim J, Haradhrava NJ, et al. The repertoire of mutational signatures in human cancer. *Nature* 2020;578:94–101.
- Li M, Shandilya SMD, Carpenter MA, et al. First-in-class small molecule inhibitors of the single-strand DNA cytosine deaminase APOBEC3G. *ACS Chem Biol* 2012;7:506–17.
- Zhou X, Du J, Wang H, et al. Repositioning liothyronine for cancer immunotherapy by blocking the interaction of immune checkpoint TIGIT/PVR. *Cell Commun Signal* 2020;18:142.
- Shi K, Carpenter MA, Kurahashi K, et al. Crystal structure of the DNA deaminase APOBEC3B catalytic domain. *J Biol Chem* 2015;290:28120–30.
- Sun Y, Qian Y, Chen C, et al. Extracellular vesicle IL-32 promotes the M2 macrophage polarization and metastasis of esophageal squamous cell carcinoma via FAK/STAT3 pathway. *J Exp Clin Cancer Res* 2022;41:145.
- Zhou X, Jiao L, Qian Y, et al. Repositioning azelnidipine as a dual inhibitor targeting CD47/SIRPα and TIGIT/PVR pathways for cancer immuno-therapy. *Biomolecules* 2021;11. doi:10.3390/biom11050706. [Epub ahead of print: 10 05 2021].
- Shi K, Carpenter MA, Banerjee S, et al. Structural basis for targeted DNA cytosine deamination and mutagenesis by APOBEC3A and APOBEC3B. *Nat Struct Mol Biol* 2017;24:131–9.
- Coticello SG, Thomas CJF, Petersen-Mahrt SK, et al. Evolution of the AID/APOBEC family of polynucleotide (deoxy)cytidine deaminases. *Mol Biol Evol* 2005;22:367–77.
- Hakata Y, Miyazawa M. Deaminase-independent mode of antiretroviral action in human and mouse APOBEC3 proteins. *Microorganisms* 2020;8. doi:10.3390/microorganisms8121976. [Epub ahead of print: 12 12 2020].
- Gao Y-B, Chen Z-L, Li J-G, et al. Genetic landscape of esophageal squamous cell carcinoma. *Nat Genet* 2014;46:1097–102.
- Chen Z, Yao N, Zhang S, et al. Identification of critical radioresistance genes in esophageal squamous cell carcinoma by whole-exome sequencing. *Ann Transl Med* 2020;8:998.
- Mangalparthi KK, Patel K, Khan AA, et al. Mutational landscape of esophageal squamous cell carcinoma in an Indian cohort. *Front Oncol* 2020;10:1457.
- Park HL, Kim MS, Yamashita K, et al. DCC promoter hypermethylation in esophageal squamous cell carcinoma. *Int J Cancer* 2008;122:2498–502.
- Codipilly DC, Qin Y, Dawsey SM, et al. Screening for esophageal squamous cell carcinoma: recent advances. *Gastrointest Endosc* 2018;88:413–26.
- Vesely MD, Chen L. Normalization cancer immunotherapy for melanoma. *J Invest Dermatol* 2020;140:1134–42.
- Chang J, Tan W, Ling Z, et al. Genomic analysis of oesophageal squamous-cell carcinoma identifies alcohol drinking-related mutation signature and genomic alterations. *Nat Commun* 2017;8:15290.
- Mao Y, Lv M, Zhang Y, et al. APOBEC3B expression and its prognostic potential in breast cancer. *Oncol Lett* 2020;19:3205–14.
- Xia S, Gu Y, Zhang H, et al. Immune inactivation by APOBEC3B enrichment predicts response to chemotherapy and survival in gastric cancer. *Oncimmunology* 2021;10:1975386.
- Venkatesan S, Angelova M, Puttick C, et al. Induction of APOBEC3 exacerbates DNA replication stress and chromosomal instability in early breast and lung cancer evolution. *Cancer Discov* 2021;11:2456–73.
- Li G, Lou H-X. Strategies to diversify natural products for drug discovery. *Med Res Rev* 2018;38:1255–94.
- Luo F, Gu J, Chen L, et al. Systems pharmacology strategies for anticancer drug discovery based on natural products. *Mol Biosyst* 2014;10:1912–7.
- Peng L-Q, Yu W-Y, Xu J-J, et al. Pyridinium ionic liquid-based liquid-solid extraction of inorganic and organic iodine from laminaria. *Food Chem* 2018;239:1075–84.

- 53 Nelson SM, Gao Y-T, Nogueira LM, *et al.* Diet and biliary tract cancer risk in Shanghai, China. *PLoS One* 2017;12:e0173935.
- 54 Skibola CF, Curry JD, VandeVoort C, *et al.* Brown kelp modulates endocrine hormones in female sprague-dawley rats and in human luteinized granulosa cells. *J Nutr* 2005;135:296–300.
- 55 Feldt-Rasmussen U. Iodine and cancer. *Thyroid* 2001;11:483–6.
- 56 Aydin EM, Demir TD, Seymen N, *et al.* The crosstalk between H. pylori virulence factors and the PD1:PD-L1 immune checkpoint inhibitors in progression to gastric cancer. *Immunol Lett* 2021;239:1–11.
- 57 Ries J, Agaimy A, Wehrhan F, *et al.* Importance of the PD-1/PD-L1 axis for malignant transformation and risk assessment of oral leukoplakia. *Biomedicines* 2021;9. doi:10.3390/biomedicines9020194. [Epub ahead of print: 16 02 2021].
- 58 Mascaux C, Angelova M, Vasaturo A, *et al.* Immune evasion before tumour invasion in early lung squamous carcinogenesis. *Nature* 2019;571:570–5.
- 59 Wang J, Xie T, Wang B, *et al.* PD-1 blockade prevents the development and progression of carcinogen-induced oral premalignant lesions. *Cancer Prev Res* 2017;10:684–93.
- 60 Kennedy LB, Salama AKS. A review of cancer immunotherapy toxicity. *CA Cancer J Clin* 2020;70:86–104.
- 61 Chang AE, Golob JL, Schmidt TM, *et al.* Targeting the gut microbiome to mitigate immunotherapy-induced colitis in cancer. *Trends Cancer* 2021;7:583–93.
- 62 Haanen JBAG, Carbonnel F, Robert C, *et al.* Management of toxicities from immunotherapy: ESMO clinical practice guidelines for diagnosis, treatment and follow-up. *Ann Oncol* 2017;28:iv119–iv142.
- 63 Dahl EK, Abed OK, Kjeldsen J, *et al.* Safety and efficacy of infliximab and corticosteroid therapy in checkpoint inhibitor-induced colitis. *Aliment Pharmacol Ther* 2022;56:1370–82.
- 64 Alexander JL, Ibraheim H, Richards C, *et al.* Oral beclomethasone dipropionate is an effective treatment for immune checkpoint inhibitor induced colitis. *J Immunother Cancer* 2022;10.
- 65 Bekhet OH, Eid ME. The interplay between reactive oxygen species and antioxidants in cancer progression and therapy: a narrative review. *Transl Cancer Res* 2021;10:4196–206.
- 66 Chiorcea-Paquim A-M. 8-Oxoguanine and 8-oxodeoxyguanosine biomarkers of oxidative DNA damage: a review on HPLC-ECD determination. *Molecules* 2022;27. doi:10.3390/molecules27051620. [Epub ahead of print: 01 Mar 2022].
- 67 Barr PM, Miller TP, Friedberg JW, *et al.* Phase 2 study of imexon, a prooxidant molecule, in relapsed and refractory B-cell non-hodgkin lymphoma. *Blood* 2014;124:1259–65.
- 68 Szklener K, Szklener S, Michalski A, *et al.* Dietary supplements in chemotherapy-induced peripheral neuropathy: a new hope? *Nutrients* 2022;14. doi:10.3390/nu14030625. [Epub ahead of print: 31 Jan 2022].